AgriEngineering

Article

Varietal Identification and Yield Estimation in Potatoes Using UAV RGB Imagery in the Southern Highlands of Peru

Miguel Tueros [1], Malú Galindo [2], Jean Alvarez [1], Jesús Pozo [1], Patricia Condezo [1], Rusbel Gutierrez [1], Rolando Bautista [1], Walter Mateu [1], Omar Paitamala [3] and Daniel Matsusaka [3,*]

[1] Estación Experimental Agraria Canaán, Instituto Nacional de Innovación Agraria (INIA), Ayacucho 05002, Peru; jeshum011@gmail.com (J.P.)
[2] Dirección de Gestión de la Innovación Agraria, Instituto Nacional de Innovación Agraria (INIA), Av. La Molina 1981, Lima 15200, Peru
[3] Dirección de Investigación y Desarrollo Tecnológico, Instituto Nacional de Innovación Agraria (INIA), Av. La Molina 1981, Lima 15200, Peru; prosem@inia.gob.pe
* Correspondence: dmatsusaka@agro.uba.ar

Abstract

The cultivation of potatoes is essential for rural food security, and the use of Unmanned Aerial Vehicle Red-Green-Blue (UAV-RGB) imagery allows for precise and cost-effective estimation of yield and identification of varieties, overcoming the limitations of manual assessment. We evaluated four INIA varieties (Bicentenario, Canchán, Shulay and Tahuaqueña) by integrating agronomic measurements (height, number and weight of tubers, leaf health) with color and textural indices derived from RGB orthomosaics. Yield prediction was modeled using Random Forest (RF) and Gradient Boosting (GB); varietal identification was approached with (i) a Convolutional Neural Network (CNN) that classifies RGB images and (ii) classical models such as Random Forest, Support Vector Machines (SVMs), K-Nearest Neighbors (KNNs), Decision Trees and Logistic Regression trained on EfficientNetB0 embeddings. The results showed significant genotypic differences in yield ($p < 0.001$): Tahuaqueña 13.86 $\pm$ 0.27 t ha^{-1} and Bicentenario 6.65 $\pm$ 0.27 t ha^{-1}. The number of tubers ($r = 0.52$) and plant height ($r = 0.23$) correlated with yield; RGB indices showed low correlations ($r < 0.3$) and high redundancy ($r > 0.9$). RF achieved a better fit (Coefficient of determination, $R^2 = 0.54$; Root Mean Square Error, RMSE = 2.72 t ha^{-1}), excelling in stolon development ($R^2 = 0.66$) and losing precision in maturation due to foliar senescence. In classification, the CNN and RF on embeddings achieved F1-macro $\approx$ 0.69 and 0.66 (Receiver Operating Characteristic—Area Under the Curve, ROC AUC RF = 0.89), with better identification of Bicentenario and Shulay. We conclude that UAV-RGB is a cost-effective alternative for phenotypic monitoring and varietal selection in high Andean contexts. These findings support the integration of UAV-RGB imagery into breeding and monitoring pipelines in resource-limited Andean systems.

Keywords: phenological stages; RGB indices; random forest; convolutional neural network; gradient boosting; precision agriculture; Andean highlands

Academic Editor: Giovanni Rallo

Received: 5 November 2025
Revised: 19 December 2025
Accepted: 6 January 2026
Published: 12 February 2026

1. Introduction

Potato (*Solanum tuberosum* L.) is a globally significant crop, valued for its nutritional profile, providing 18% carbohydrates, 2.5% proteins, vitamins (especially C and B) and minerals [1]. It is also renowned for its remarkable adaptability to different altitudinal zones, originating from the Peruvian Andes [2]. Furthermore, it is a key crop for global food

security, ranking fourth in world production after maize, rice and wheat [3,4]. According to the Food and Agriculture Organization (FAO) statistics in 2023, global potato production reached a record, with 383 million tons, consolidating its status as the leading non-cereal food crop in terms of volume, with a 2% increase from 2022 to 2023 [5]. In Peru, according to the Ministry of Agricultural Development and Irrigation (MIDAGRI), the national average yield reached 17 t ha^{-1} in 2024. Notably, the locality of Ayacucho, Andean Peruvian department has reported a 37.9% yield increase in the 2023–2024 season, driven by favorable rainfall and temperature conditions [6,7]. Potato productivity can reach values between 40 and 50 t ha^{-1}, depending on the variety and the altitude at which it is cultivated [8].

Despite these yield improvements and the development of new cultivars, potato production remains highly vulnerable to climate variability, which has reduced yields of some potato varieties by up to 32% due to high temperatures, irregular rainfall and extreme weather events [9–11]. Additionally, biotic stresses remain a major constraint, as late blight (*Phytophthora infestans*) can destroy the canopy within 10–15 days, causing total crop losses [12]. Additionally, Potato virus Y (PVY) reduces yields by up to 58.84% in susceptible varieties, compared to only 5.15% in resistant ones.

To address these challenges, the National Institute of Agricultural Innovation (INIA) through its national roots and tubers program, has developed new potato cultivars specifically aimed at mitigating both biotic and abiotic stresses under Andean agroecological conditions Major biotic constraints affecting potato production include late blight [13], early blight (*Alternaria solani*) [14]., black scurf and stem canker (*Rhizoctonia solani*) [15]. In addition, key abiotic factors influencing potato crop performance in highland environments include temperature extremes, solar radiation, photoperiod, soil salinity and drought [16–19]

Among the released varieties, INIA Tahuaqueña, released by the Illpa-Puno Agricultural Experimental Station (EEA), stands out for its resistance to wart disease, smut, *Phytophthora infestans* and *Alternaria solani*, along with tolerance to drought and frost, achieving yields of up to 45 t ha^{-1} [20]. Meanwhile, the INIA-326 Shulay variety (EEA Santa Ana—Junín) shows frost tolerance and an average yield of 35 t ha^{-1} [7]. Additionally, the INIA-332 Perú Bicentenario variety (EEA Santa Ana—Junín) combines resistance to *P. infestans* and drought, along with excellent culinary quality for frying, achieving yields of up to 30 t ha^{-1} under farmers' field conditions [21]. On the other hand, the widely distributed INIA-303 Canchán variety, widely distributed in the central and southern highlands of Peru, is notable for its resistance to *P. infestans* and frost, with an average yield of 30 t ha^{-1} [22,23].

In parallel with genetic improvement efforts, advances in digital phenotyping are transforming crop monitoring and selection. Modern plant breeding integrates high-throughput phenotyping (HTP) tools, where Unmanned Aerial Vehicles (UAVs, or drones) are increasingly used to overcome the subjectivity and low repeatability of manual assessments [24,25]. The capture of high-resolution RGB images allows for precise, efficient and non-destructive monitoring of numerous plots, enabling the quantification of traits such as emergence, vigor, canopy cover and responses to biotic or abiotic stresses [24]. When combined with analytical and predictive models, UAV-derived data accelerate the identification of superior genotypes and improve yield estimation accuracy [26–28]. Overall, UAVs contribute to genetic improvement programs by integrating speed, objectivity and sustainability into agronomic decision-making [29].

The crop information obtained through UAVs also enables advanced analyses such as vegetation indices, water availability and weed identification, contributing to more efficient crop management [30–32]. RGB images offer benefits such as high spatial resolution, allowing for precise quantification of traits like emergence, canopy cover, vigor

and plant uniformity [33]. Additionally, their compatibility with machine learning models facilitates massive data processing with low computational demands [34]. The texture and color indices generated from RGB images provide reliable estimates of crop growth and physiological status, offering a practical and reproducible alternative to other imaging systems [35].

Recent research has validated the potential of UAV-RGB technology across several crops. For instance, in wheat, UAV-RGB evaluation using 22 features related to vegetation indices, color and texture enabled the construction of a highly accurate model (R^2 = 0.981), optimizing regional harvest decisions [36]. Similarly, in potato, UAV-based RGB imagery allows precise canopy assessment across nitrogen levels, enabling dynamic tracking of biomass accumulation and yield prediction [37]. This multitemporal approach captures the phenological changes, allowing for more precise mapping and monitoring, which is crucial for precision agriculture [35]. Studies integrating UAV-RGB images with Random Forest classification algorithms have achieved high accuracy (r^2 = 0.96) in estimating potato emergence, providing an objective and efficient phenotyping tool for fertilizer management [38]. Moreover, recent studies have demonstrated that the use of RGB images combined with vegetation indices and texture features extracted using Gray Level Co-occurrence Matrix (GLCM) and Gabor filters (multiscale wavelet) improved the estimation of potato aerial biomass [39], establishing more robust relationships with crop yield.

Machine learning techniques play a pivotal role in extracting actionable information from UAV-RGB imagery. Random Forest (RF) models are particularly robust against noise and overfitting, capable of handling correlated variables while providing interpretable results. This model surpasses other approaches in its ability to generalize and select variables, also generating importance rankings that reveal key phenotypic traits in potato cultivation [26,40]. Complementarily, deep convolutional neural networks (CNNs) enable the segmentation of RGB images obtained by UAVs to detect plants, count individuals and identify vegetation cover, thus optimizing the automated analysis of crop growth and development [41]. Collectively, algorithms such as CNN, Random Forest, XGBoost and SVM have been successfully applied to image analysis in precision agriculture, enhancing the early identification of patterns associated with yield and crop response to different environmental factors [42,43]. While CNNs are effective in varietal identification by extracting complex canopy traits, they require large volumes of data and high computational capacity [44]. By contrast, XGBoost and SVM offer specific advantages such as the ability to model complex nonlinear relationships, handle high dimensionality and perform well with imbalanced data when sampling techniques are used, yet Random Forest remains advantageous for its balance between accuracy, robustness and interpretability [45].

Despite these advances, few studies have applied CNNs to UAV-RGB imagery for in-field potato varietal identification over the past five years primarily because RGB sensors capture only three spectral bands, limiting subtle phenotypic differentiation [46]. Nevertheless, their affordability and accessibility make them a highly practical alternative to multispectral or hyperspectral sensors, particularly where advanced technology access is limited [47,48]. In this context, If RGB-based models achieve robust and statistically validated performance, they offer an optimal cost–benefit approach, even though maximum discrimination is achieved using hyperspectral or VNIR (visible and near-infrared spectrum) sensors.

Potato cultivation remains strategically vital across the Andes, especially in Peru, serving as both a nutritional and economic cornerstone for thousands of rural communities. However, manual evaluation of yield and crop vigor remains labor-intensive, subjective and limited in spatial coverage. In this context, UAV-RGB imagery combined with machine

learning models offers a scalable and cost-effective for objective phenotypic assessment under Andean conditions.

Therefore, the objectives of this study were to (i) predict potato yield across four key phenological stages using Random Forest (RF) and Gradient Boosting (GB) models and to compare their predictive performance using the coefficient of determination (R^2) and root mean square error (RMSE); (ii) identify the optimal phenological window for UAV-RGB data acquisition that maximizes yield, and (iii) evaluate and compare varietal identification strategies based on convolutional neural networks (CNNs) in contrast to EffcientNetBo embeddings combined with classical machine learning classifiers, using macro-averaged F1 score and area under the ROC curve (AUC) as performance. Ultimately this work aims to provide operational guidelines for integrating UAV-RGB imagery into potato breeding and monitoring programs in high Andean agroecosystems.

2. Materials and Methods

2.1. Characteristics of the Study Area and Experimental Design

The study was conducted during the 2024–2025 growing season on a 390 m^2 plot located in Viscachayocc (74°12′7″ W, 13°4′48″ S; 2727 m a.s.l.), belonging to the Canaán Agricultural Experimental Station (INIA), situated in the district of Andrés Avelino Cáceres Dorregaray, province of Huamanga, Ayacucho, Peru (Figure 1).

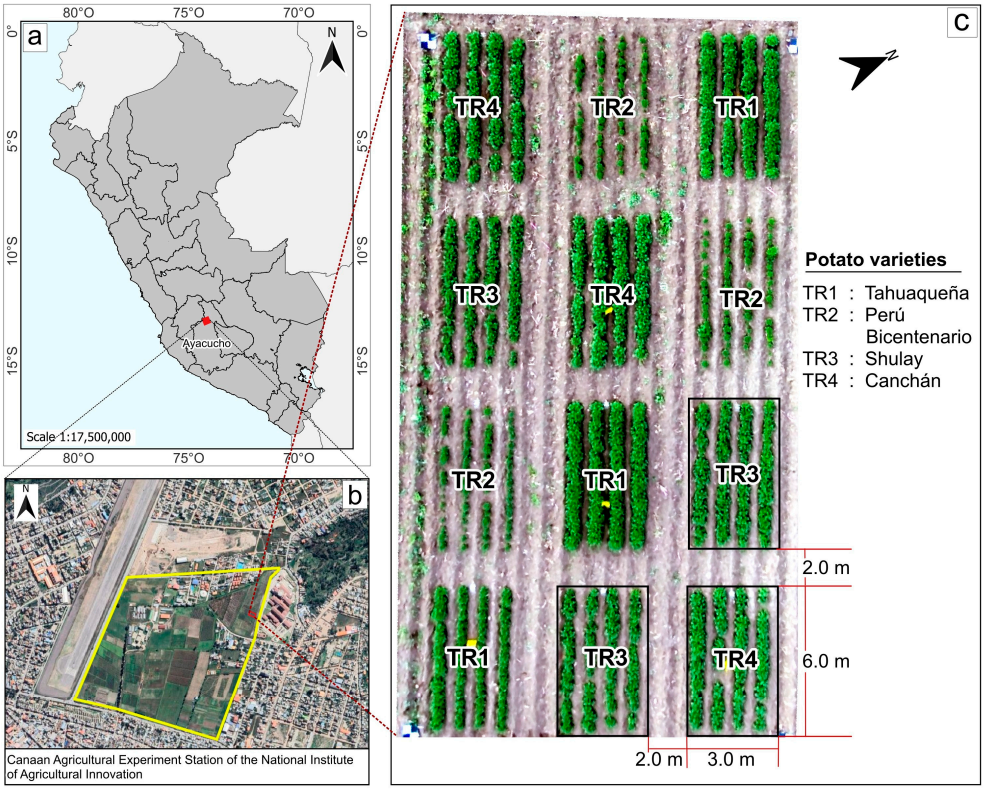

Figure 1. Geographic location of the experimental sites in the Ayacucho region, Peru (scale 1:17,500,000) (**a**). The gray area represents the Previian territory and the red pint indicates the location of the Canaán Experimental Agricultural Station (EEA Canaán) of the National Institute of Agricultural Innovation (INIA) (**b**). RGB orthomosaic of the experimental field showing the cultivation of four potato varieties: TR1 (Tahuaqueña), TR2 (Perú Bicentenario), TR3 (Shulay), and TR4 (Canchán), during the 2024–2025 cropping season (**c**).

The study area exhibited moderate thermal variation. Average air temperature decreased from 17.6 °C to 15.5 °C, with extremes ranging from 8.8 °C to 28.9 °C. Relative

humidity increased from 54.7% to 78.6%, while precipitation averaged 1.1 mm h^{-1}, reaching peaks of 96 mm h^{-1} during intense events. Solar radiation gradually decreased from 247.3 to 184 W m^{-2}, with maximum values between 983 and 1178 W m^{-2}, indicating high photosynthetic potential. Meteorological data were obtained from the INIA-Canaán weather station, which operates under the supervision of National Meteorology and Hydrology Service of Peru (SENAMHI).

The experiment employed a randomized complete block design (RCBD) with 4 treatments represented by the varieties (Tahuaqueña, Perú Bicentenario, Shulay and Canchan), generating 3 repetitions and totaling 12 experimental units (EUs). The individual plots measured 18 m^2 (4 rows of 6 m long spaced 1 m between rows and 0.30 m between planting holes, accommodating 84 plants).

2.2. Soil Physicochemical Characterization

Before the establishment of the experiment, composite soil samples were collected from a depth of 0–40 cm. These samples were sealed and transported to the Soil, Water and Foliar Laboratory (LABSAF) at the Canaán Agricultural Experiment Station (INIA) for analysis. In the laboratory, key physicochemical parameters were determined, including texture, pH [49], electrical conductivity (EC) [50], organic matter (OM) [51], and total nitrogen (N) [52]. In addition, cation exchange capacity (CEC), available phosphorus (P) and exchangeable potassium (K) were evaluated [53,54] (Table 1).

Table 1. Physicochemical characteristics of the soil before the establishment of the potato experiment.

Variable	Unit	Result
Sand	%	26.73
Silt	%	29.6
Clay	%	43.67
Texture	_	Clay loam soil
pH	_	7.2
Electrical conductivity (EC)	dS m^{-1}	17.3
Organic matter (OM)	%	2.2
Nitrogen (N)	%	0.11
Phosphorus (P)	Ppm	29.5
Potassium (K)	Ppm	422.5
Calcium (Ca)	Cmol (+)·kg^{-1}	48.5
Magnesium (Mg)	Cmol (+)·kg^{-1}	10.75
Potassium (K)	Cmol (+)·kg^{-1}	2.64
Sodium (Na)	Cmol (+)·kg^{-1}	0.51
Cation exchange capacity (CEC)	Cmol (+)·kg^{-1}	62.41

To ensure analytical accuracy, all measurements were performed using certified and calibrated laboratory equipment. Soil pH and electrical conductivity were measured using a benchtop pH meter (WTW INOLAB, model pH 7310, Xylem Analytics, Weilheim, Germany) and a conductivity meter (WTW INOLAB, model Cond 7310, Xylem Analytics, Weilheim, Germany), respectively. Organic matter content was quantified using a digital burette (BDeco, model DCB5000, Boeckel, Hamburg, Germany). Soil texture analysis employed a hydrometer (THERMCO ASTM, model 152H, HB Instrument/Gilson Company Inc., Trappe, PA, USA) and a mechanical disperser (Hamilton Beach, model HMD400, Reno, NV, USA). Total nitrogen was measured using a digestion system (BERT, model Heizblock K24, Heizbiac GmbH, Ulm, Germany) followed by distillation with a Destillere 52 unit (WESDOM Group, Wenzhou, China). Available phosphorus was determined using a spectrophotometer (Thermo Scientific, model Genesys 150, Rochester, NY, USA), while exchangeable bases and potassium were measured using an atomic emission

spectrometer (Agilent Technologies, model 4210, Santa Clara, CA, USA). Mass determinations were carried out using an analytical balance (Bell, model M214Ai, BEL Engineering, Monza, Italy).

2.3. Plant Material, Crop Management and Fertilization

Four INIA-released potato varieties were used: INIA-Tahuaqueña, INIA-332 Perú Bicentenario, INIA-326 Shulay and INIA-303 Canchán. Certified seed tubers of each variety were planted on 12 November 2024, with two tubers per planting hole and 0.30 m spacing between plants.

At planting, base fertilization consisted of Terrasur organic fertilizer (5000 kg ha^{-1}), a rate within the range recommended for improving soil structure and nutrient availability in potato production systems [55]. Nitrogen was supplied as urea (350 kg ha^{-1}), applied in two equal doses (50% at planting and 50% at the first hilling), following standard agronomic practices reported for potatoes [56]. Phosphorus was applied as diammonium phosphate (400 kg ha^{-1}) [57], and potassium as potassium chloride (200 kg ha^{-1}) [58], consistent with commonly recommended fertilization levels for potato cultivation. Prior to treatment establishment, a soil analysis was conducted to characterize initial soil fertility and ensure uniform fertilizer application across all experimental plots.

For pest management, alpha-cypermethrin (60 mL/20 L) was applied against *Epicauta* spp., *Phthorimaea operculella* and *Epitrix* spp. For disease control, preventive biocontrol applications of *Bacillus subtilis* and *Trichoderma viride* (40 g per 20 L of water) were used against *Phytophthora infestans* [59,60]. The crop was harvested 135 days after sowing (DAS).

2.4. Agronomic Yield Evaluations of Potato Varieties Developed by INIA

Agronomic data collection was performed at key phenological stages of potato development for all four varieties. Between 30 and 45 DAS, the number of emerged plants per row was recorded, along with counts of healthy and damaged leaves.

At 45, 60, 75, 90 and 108 DAS, plant height was measured using a wooden ruler from the base to the apex of the apical meristem, without stretching or compressing, Measurements were taken from six plants per row (two at the beginning, two in the middle and two at the end), totaling 24 plants per experimental unit. In Addition, a count of healthy leaves (without damage from pests or diseases) and affected leaves was performed, complemented by aerial monitoring using UAV (Figure 2).

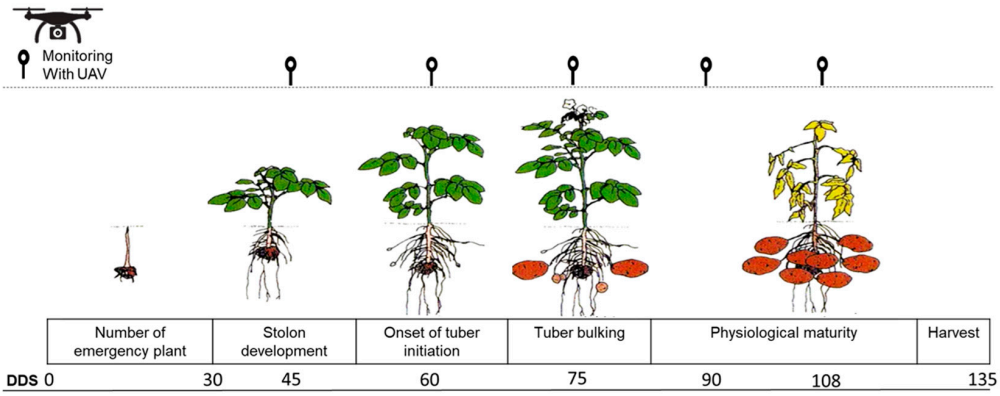

Figure 2. Phenological stages of potato development during the 2024–2025 cropping season and UAV monitoring schedule. The diagram illustrates the main growth stages: emergence, stolon development, onset of tuber initiation, tuber bulking, physiological maturity and harvest, corresponding to 0–135 days after sowing (DAS).

At 135 DAS, morphophysiological attributes such as the number and weight of tubers per plant were evaluated using an ACCULAB ALC-6100.1 g precision balance, from the same 24-plant sampling per EU. These data were used to determine yield per experimental unit.

2.5. Statistical Analysis of Agronomic Data

All experimental field datasets were processed using RStudio (v.2024.12.1 + 563). An initial exploratory data analysis was conducted with the dplyr package [61]. The normality and homoscedasticity of each response variable were assessed using the Shapiro–Wilk and Levene tests, respectively. Since several traits did not meet one or both assumptions, a robust analysis of variance (ANOVA) was performed using the WRS2 package [62]. For mean comparisons, Sidak adjustment was applied through the RHSD function to control Type I error and obtain corrected confidence intervals [63].

2.6. Methodological Framework

The methodological framework integrates UAV-acquired data and field measurements for yield prediction (a) and varietal identification (b) (Figure 3).

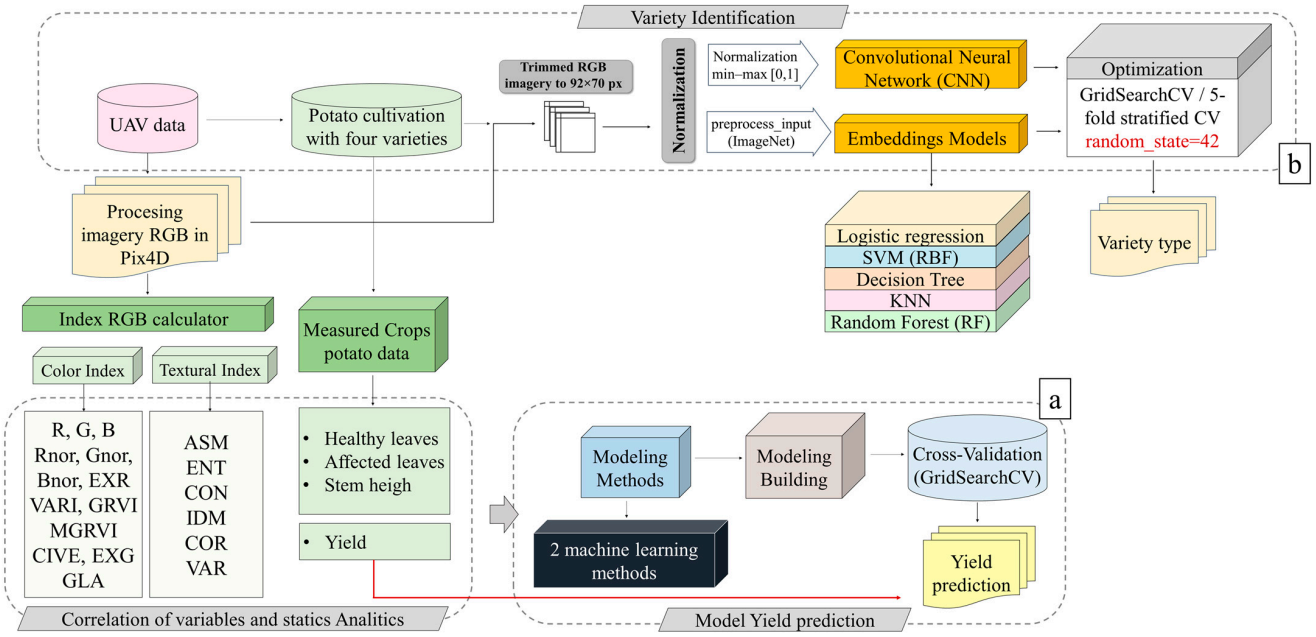

Figure 3. Workflow designed for predicting potato crop yield and variety identification based on data collected during the 2024–2025 agricultural campaign: (**a**) workflow describing the complete process for potato yield prediction (**b**) potato variety discrimination.

In component (a), six textural indices and thirteen color indices derived from RGB image processing were integrated with field-based agronomic data (e.g., yield, stem height and leaf health). These variables were used to build a correlation matrix, enabling the identification of the indices most strongly associated with the phenotypic and productive traits of interest [40,64]. Two machine learning algorithms, Random Forest (RF) and Gradient Boosting (GB)—were implemented to predict yield and the model optimization was achieved through GridSearchCV cross-validation to enhance generalization and accuracy.

In component (b), a variety identification model was developed using Convolutional Neural Networks (CNNs) and additional classification algorithms including Logistic Regression, Support Vector Machine (SVM, RBF kernel), Decision Tree, K-Nearest Neighbors (KNN) and Random Forest (RF). For non-CNN models, embeddings derived from CNN feature extraction were utilized to improve classification accuracy.

2.7. UAV Data Acquisition and Processing

Data collection was conducted through UAV flights using a utilizing a DJI Phantom 4 drone equipped with an RGB imaging system, real-time kinematic (RTK) module and TimeSync for temporal synchronization. The RGB sensor comprised three cameras covering the blue (450 nm ± 16 nm), green (560 nm ± 16 nm) and red (650 nm ± 16 nm) bands, each with a resolution of 2 MP and a global shutter, mounted on a 3-axis stabilized gimbal. To enhance geospatial accuracy, differential GPS surveying was employed, recording UTM coordinates across four control grids as illustrated in Figure 4. Flights were conducted at noon under clear skies, at an altitude of 20 m, in manual mode, capturing images at a resolution of 2.356 cm/pixel every 4 s [40].

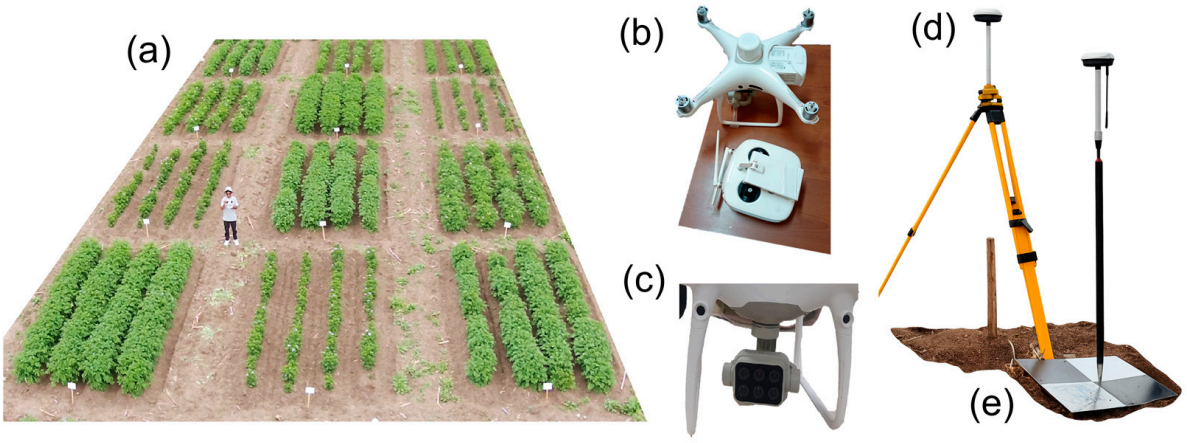

Figure 4. (**a**) Study area; (**b**) UAV; (**c**) RGB sensor; (**d**) Tripod and differential GPS; and (**e**) Ground control point.

Six flights were performed at 45, 60, 75, 90 and 108 days after sowing (DAS), corresponding to the phenological stages of the potato crop: vegetative growth, maximum canopy development, tuber filling, onset of senescence and maturity. Each flight enabled the recording of crop vigor variations, thereby optimizing yield prediction and constructing time series capable of characterizing the phenological transitions of the potato crop, following previously described methodologies [65–67]. The average flight duration per route was approximately 6 min and 30 s. Optimal climatic conditions were identified between 11 a.m. and 2 p.m., during when solar radiation is stable, and the angular incidence of light allows for homogeneous capture of canopy reflectance, minimizing radiometric errors associated with light variations [68]. This strategic timing ensures the reliability and accuracy of the data collected, facilitating robust analysis and interpretation of the crop's phenological and productive parameter.

2.7.1. Image Preprocessing

The preprocessing of the images was carried out using the photogrammetric software Pix4Dmapper Pro (Pix4D S.A., Prilly, Lausanne, Switzerland), which enabled the generation of georeferenced orthomosaics and digital surface models (DSM). The RGB orthomosaics obtained via UAV were utilized for two main purposes: variety identification and yield estimation. For the first case, the images were segmented into 92 × 70-pixel clips, centered on the area with the highest proportion of the potato plant. In the second case, the RGB orthomosaics were processed using a segmentation method based on the ExG vegetation index, as this index has demonstrated superior performance in separating the canopy from the soil [36]. This methodology allowed for the generation of specific vegetation masks for

each variety and treatment, which facilitated the precise delimitation of the aerial biomass of the potato crop, as well as the extraction of RGB indices for each mask (Figure 5).

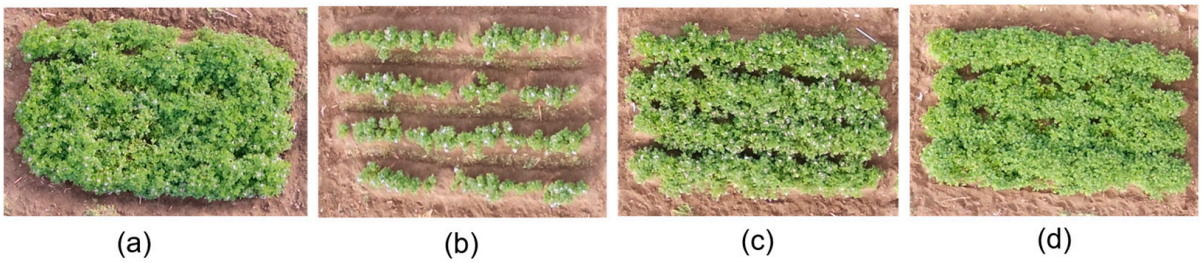

Figure 5. Vegetation mask generation for potato varieties: (**a**) INIA-Tahuaqueña, (**b**) INIA-332 Perú Bicentenario, (**c**) INIA-326 Shulay, and (**d**) INIA-303 Canchan. The imagery corresponds to 60 days after sowing (60 DAS).

All RGB images were additionally subjected to a cropping procedure to extract regions of interest with a fixed size of 92 × 70 pixels. This approach preserves the original spatial geometry and relative proportions of plant structures, avoiding distortions associated with interpolation-based rescaling. The cropped images were subsequently normalized to the [0–1] range using min–max scaling by dividing pixel intensities by 255 through the ImageDataGenerator framework. To enhance model robustness and mitigate the limited spatial scale of the experiment, data augmentation techniques were applied during CNN training, including rotations (±10°), zoom (0.1), horizontal flipping, and small spatial translations, simulating realistic variations in UAV flight altitude, image resolution, and viewing perspective. For models based on EfficientNetB0, the official ImageNet preprocess_input function was employed to ensure consistency with pretrained network requirements. When EfficientNetB0-derived embeddings were used as input for classical machine learning classifiers, the extracted features were already represented in the corresponding normalized feature space.

These preprocessing and data augmentation strategies were specifically implemented to account for potential variations in image resolution, flight altitude, and object perspective, thereby improving model robustness under different UAV acquisition conditions.

2.7.2. Color and Textural Indices Derived from RGB Images

From the RGB images, color and texture indices were calculated to monitor biomass, growth and crop vigor, following previous approaches that associate these indices with a robust canopy structure [69–71]. In alignment with these methodologies, color indices (CI) were generated through the normalization of the RGB bands (Table 2), while textural indices (TI) were obtained using the gray-level co-occurrence matrix (GLCM) approach [72,73]. The processing was conducted in QGIS version 3.42-Münster, utilizing the r.texture module from the GRASS texture plugin for the TI [74].

These indices were calculated based on the probability p(i,j) of occurrence of pixel pairs (i,j), where i and j correspond to the gray levels within a specified window and the coordinates of the co-occurrence matrix. The parameter N_g represents the number of unique gray levels present in the quantified image, while μ and σ denote the mean and standard deviation of p(i,j), respectively. Both CI and TI were employed as input variables for the yield prediction model.

Table 2. Index imagery RGB.

Type	Index	Meaning	Formula	References
Color Indices	R	Red reflectance	R = R	[75]
	G	Green reflectance	G = G	[75]
	B	Blue reflectance	B = B	[75]
	Rnor	Normalized red reflectance	r = R/(R + G + B)	[75]
	Gnor	Normalized green reflectance	g = G/(R + G + B)	[75]
	Bnor	Normalized blue reflectance	b = B/(R + G + B)	[75]
	EXR	Excess-red index	EXR = 1.4 r − g	[76]
	VARI	Vegetation atmospherically resistant index	VARI = (g − r)/(g + r − b)	[77]
	GRVI	Green-red vegetation index	GRVI = (g − r)/(g + r)	[78]
	MGRVI	Modified green-red vegetation index	MGRVI = $(g^2 - r^2)/(g^2 + r^2)$	[78]
	CIVE	Color index of vegetation	CIVE = 0.441 r − 0.881 g + 0.385 b + 18.78745	[79]
	EXG	Excess-green index	EXG = 2 g − b − r	[80]
	GLA	Green leaf algorithm index	GLA = (2G − B − R)/(2G + B + R)	[81]
Textural Indices	ASM	Angular Second Moment	$\sum_i \sum_j p(i,j)^2$	[82,83]
	ENT	Entropy	$-\sum_i \sum_j p(i,j)\log(p(i,j))$	[84]
	CON	Contrast	$\sum_{n=0}^{N_g-1} n^2 \left\{ S \sum_{j=1}^{N_g-1} \sum_{j=1}^{N_g-1} p(i,j) \right\}$	[82,83]
	IDM	Inverse Difference Moment	$\sum_i \sum_j \frac{1}{1+(i-j)^2} p(i,j)$	[85]
	COR	Correlation	$\frac{\sum_j p\left(ij\left(p(i,j)-u_x u_y\right)\right.}{\sigma_x \sigma_y}$	[84,85]
	VAR	Variance	$\sum_i \sum_j (i-u)^2 p(i,j)$	[84,85]

2.8. Modeling Methods

2.8.1. Potato Crop Yield Modeling

The regression algorithms employed range from simple approaches to advanced ensembles such as Random Forest (ensemble of tree bagging) and Gradient Boosting (classic boosting ensemble). The Random Forest (RF) is a widely used machine learning model in agriculture for forecasting yield and managing crops. This model generates multiple decision trees from random subsets of the original dataset and then combines the predictions from these trees to improve accuracy and reduce the risk of overfitting. The robustness of RF makes it particularly effective in addressing the variability of agricultural data and providing reliable predictions on crop yield, soil conditions, and pest or disease detection [86–88]. Gradient Boosting is an ensemble method that sequentially builds weakly predictive trees by correcting the errors of the previous model, achieving high accuracy and good fit in non-linear relationships. In agriculture and remote sensing, it has demonstrated effectiveness in yield estimation [89–91].

2.8.2. Modeling for Variety Identification

This stage focused on potato variety identification using RGB imagery. A deep learning approach based on a convolutional neural network (CNN) was implemented for direct image classification. In parallel, a hybrid framework was developed to compare CNN performance with classical machine learning classifiers trained on feature embeddings generated by EfficientNetB0, pre-trained on ImageNet.

All RGB images were cropped into fixed-size patches of 92 × 70 pixel, preserving the original spatial geometry. For the CNN trained end-to-end, pixel intensities were normalized to the [0–1] range by dividing each RGB channel by 255. In contrast, for EfficientNetB0-based models, the official preprocess_input function was applied, implementing the standard ImageNet normalization required for pretrained convolutional net-

works. To improve model robustness, for the CNN-based approach, data augmentation techniques were applied, including rotations ($\pm 10^{\circ}$), zoom (0.1), horizontal flipping, and minor translations.

Hyperparameter Optimization and Cross-Validation

Classical machine learning models were optimized using RandomizedSearchCV, which provides a computationally efficient alternative to exhaustive grid search in large hyperparameter spaces. Model evaluation was performed using stratified five-fold cross-validation (StratifiedKFold, n_splits = 5, shuffle = True), ensuring that class proportions were preserved in each fold. To guarantee reproducibility, random seeds were fixed across all stochastic processes (random_state = 42), including fold generation and classifier initialization where applicable.

Although some class imbalance among varieties was present, explicit resampling techniques (e.g., SMOTE or undersampling) were not applied to the embeddings. Instead, the combination of data augmentation in the CNN and the evaluation of class weighting strategies (class_weight = "balanced") in compatible classifiers effectively mitigated imbalance effects without altering the original data distribution.

CNN Training Configuration

The CNN was trained using a batch size of 32 for a maximum of 100 epochs. The Adam optimizer was employed with an initial learning rate of 0.001. To prevent overfitting, early stopping was implemented by monitoring validation loss with a patience of 10 epochs and restoring the best-performing model weights. Additionally, a ReduceLROnPlateau scheduler was used (factor = 0.5, patience = 5) to automatically decrease the learning rate when validation performance plateaued.

Model performance was evaluated using accuracy, precision, recall, macro-averaged F1-score, and confusion matrices to analyze class-wise errors. EfficientNetB0 embeddings served as input features for the following classifiers:

Random Forest (RF): An ensemble learning method based on bagging, which reduces variance and performs well with noisy and multicollinear data. It provides variable importance measures useful for interpreting spectral–temporal predictions in UAV imagery. RF has shown excellent performance in crop classification and phenotypic trait estimation [88].

Support Vector Machine (SVM): A classifier that seeks the maximum-margin hyperplane in a kernel-transformed feature space. It performs effectively with extracted feature sets and moderate sample sizes, controlling overfitting through the regularization parameter C and kernel curvature γ. It is widely used for stress detection and leaf-level classification [92].

Decision Tree (DT): A recursive partitioning model that generates interpretable decision rules per node, useful for rapid diagnosis and analysis of explanatory variables. Although sensitive to overfitting, it is efficient and easily integrated into geospatial workflows [89].

K-Nearest Neighbors (KNN): A proximity-based, non-parametric method that classifies samples according to the majority of their nearest neighbors in the feature space. It effectively exploits local similarity in embeddings or spectral indices, though its performance may degrade in high-dimensional spaces without dimensionality reduction [93].

Logistic Regression (LR): A probabilistic linear classifier that estimates class membership through a logistic function. It is robust, interpretable and efficient for balanced datasets or after feature transformation and is often used as a baseline for comparing more complex models [94].

The optimized parameters included maximum tree depth, minimum number of samples per split and per leaf, regularization coefficient (C), number of neighbors and weight function.

2.9. Model Validation

2.9.1. Model Validation for Yield Prediction

In predictive studies of agricultural yield based on UAV data, a coefficient of determination (R^2) ranging from 0.5 to 0.7 is considered statistically acceptable, as spatial validation and the spectral limitations of RGB cameras can reduce the fit without significantly affecting the operational predictive capability of the model [64,95,96]. The root mean square error (RMSE) represents the average magnitude of errors, penalizing larger deviations more heavily by squaring the differences between observed and predicted values. Meanwhile, the mean absolute error (MAE) quantifies the average error of predictions and is more robust against outliers than RMSE [64].

It is important to note that the prediction of potato yield using UAV-based RGB imagery is subject to inherent biophysical and phenological limitations. Unlike aboveground crops, the economically relevant organ in potato (the tuber) develops belowground, and therefore yield estimation relies indirectly on canopy-related information. Spectral saturation during peak biomass and reduced canopy sensitivity during senescence further constrain the ability of single-sensor RGB imagery to capture yield variability, which explains why moderate R^2 values (typically between 0.4 and 0.7) are commonly reported in the literature and remain operationally useful [97,98].

First, this work provides field-based validation under high-altitude Andean conditions in southern Peru, a production system that is underrepresented in the current literature. The phenological response of potato and the canopy–tuber relationship in these environments differ from lowland systems, and local validation enhances the transferability of UAV-based models for breeding and management programs in the Ayacucho region.

Second, this study integrates varietal identification and yield estimation using the same RGB orthomosaics, whereas most previous studies address these tasks separately. This combined framework leverages genotype–phenotype covariance and offers a practical tool for prioritizing targeted sampling and decision-making in potato breeding programs operating under limited resources [99].

Third, the temporal analysis revealed a phenology-dependent predictive performance, with Random Forest models achieving higher R^2 values during the stolon development stage and reduced accuracy during maturation due to foliar senescence. This phenological insight provides an operational recommendation regarding the optimal timing of UAV flights when maximizing yield–canopy correlation is desired, a topic that has not been sufficiently explored in previous UAV-RGB potato studies [97].

2.9.2. Model Validation for Variety Identification

The identification of four potato varieties was approached using two complementary strategies. (1) A convolutional neural network (CNN) with RGB input (92 × 70 px, batch size = 16) was evaluated using Accuracy, which measures the proportion of correct classifications (ideal value = 1.0), and macro-F1, a more robust indicator in the presence of class imbalance [95,100]. (2) Classical models Random Forest, SVM, Decision Tree, KNN and Logistic Regression—were trained on embeddings extracted from EfficientNetB0, optimized through GridSearchCV (k = 5).The Accuracy, F1-macro and ROC AUC OvR metrics were used to assess model stability and multiclass discriminative ability, considering values above 0.8 as indicative of good varietal separation [101].

3. Results

3.1. Phenotypic Evaluations of Potato Varieties

The vertical vegetative development of the four potato varieties (Bicentenario, Canchan, Shulay and Tahuaqueña) was monitored over five sampling dates. A general trend of increasing stem height was observed for all varieties. The Tahuaqueña variety consistently exhibited the greatest plant height across all evaluation dates, showing a statistically significant difference from the others, and reaching 85 cm during the senescence phase. In contrast, Bicentenario (63.4 cm) and Shulay (66.15 cm) displayed the lowest values at the same stage, indicating lower vegetative vigor.

Additionally, the proportion of healthy leaves (HL) and affected leaves (AL) was analyzed for each variety. Bicentenario (AL = 234.34 leaves) and Tahuaqueña (AL = 230.34 leaves) consistently maintained more than 90% of healthy leaves at 90 days after emergence (DAE), while the Canchan variety showed a higher number of affected leaves, particularly at 45 DAE (AL = 111.64 leaves) and 60 DAE (AL = 105.07 leaves), respectively (Figure 6).

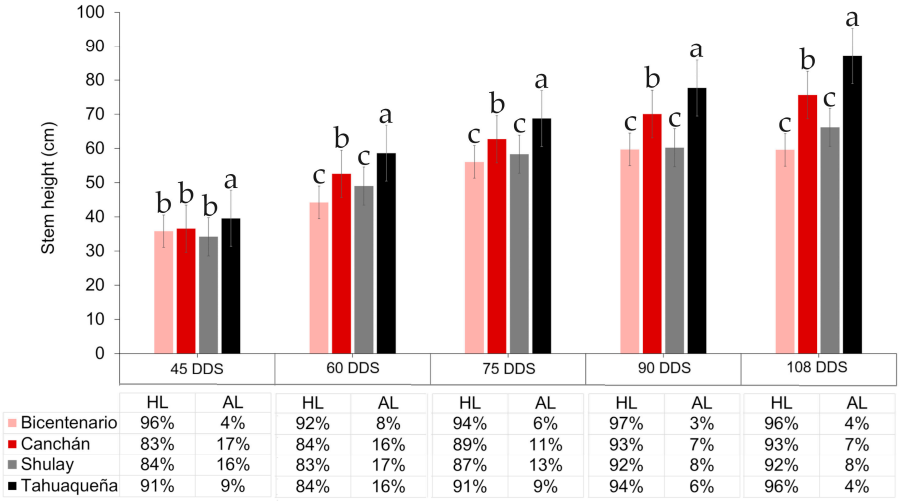

	45 DDS		60 DDS		75 DDS		90 DDS		108 DDS	
	HL	AL	HL	AL	HL	AL	HL	AL	HL	AL
Bicentenario	96%	4%	92%	8%	94%	6%	97%	3%	96%	4%
Canchán	83%	17%	84%	16%	89%	11%	93%	7%	93%	7%
Shulay	84%	16%	83%	17%	87%	13%	92%	8%	92%	8%
Tahuaqueña	91%	9%	84%	16%	91%	9%	94%	6%	96%	4%

Figure 6. Agronomic variables measured in the four monitored potato varieties. HL = % of healthy leaves relative to the total; AL = % of affected leaves relative to the total. Different letters above boxes indicate statistically significant differences among varieties at $p < 0.05$, according to Tukey's honestly significant difference (HSD) test.

3.2. Productive Yield of Varieties (t ha^{-1})

The ANOVA revealed highly significant differences among varieties ($F = 164.23$; $p < 0.001$), with a large effect size ($\eta^2 = 0.74$; 95% CI: 0.64–0.78), indicating that the varieties were clearly distinct from one another. This effect size indicated that approximately 74% of the total variability in yield was explained by genotypic factors, underscoring the strong influence of genetic differences on productivity.

Post hoc comparisons using Šidák correction further supported the presence of significant differences among varieties, identifying three statistically distinct groups. The Tahuaqueña variety exhibited the highest average yield (13.86 ± 0.27 t ha^{-1}), followed by Canchan (10.34 ± 0.27 t ha^{-1}) and Shulay (10.49 ± 0.27 t ha^{-1}), which did not differ significantly from each other and represented intermediate yield levels. In contrast, Bicentenario showed the lowest yield (6.65 ± 0.27 t ha^{-1}).

A similar pattern was observed for the total number of tubers per variety. Once again, Tahuaqueña achieved the highest average production (21 ± 7.59 tubers per plant), confirming its agronomic superiority in both yield and tuber number. Canchan (19 ± 6.32 tubers) and Shulay (15 ± 6.44 tubers) occupied intermediate positions, while Bicentenario recorded

the lowest value (9 ± 3.93 tubers), producing less than half of what was observed in Tahuaqueña (Figure 7).

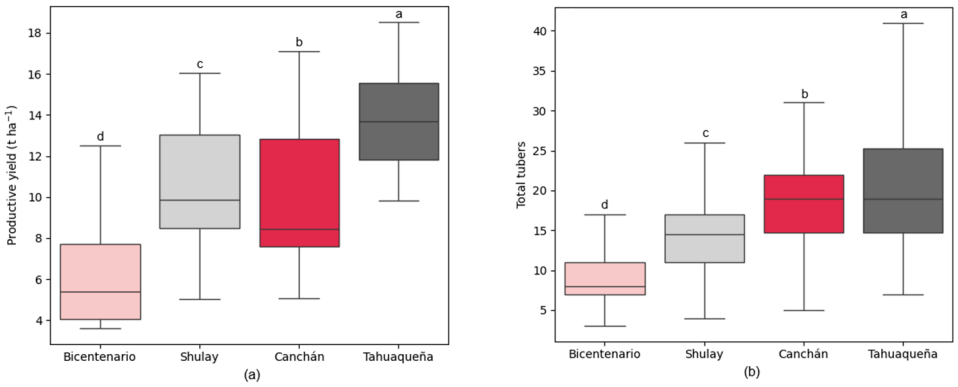

Figure 7. Variation in (**a**) productive yield (t ha^{-1}) and (**b**) total tuber number among four potato variety. Different letters in above boxes indicate statistically significant differences among varieties at $p < 0.001$), according to Tukey's honestly significant difference (HSD) test.

3.3. Correlation Analysis

The Pearson correlation analysis revealed variations in both magnitude and direction depending on the variety, highlighting positive associations of yield with the total number of tubers, plant height and the greenness indices EXG and Gnor. In the Bicentenario variety, the total number of tubers showed the strongest correlation with yield ($r = 0.42$), followed by the color indices EXG, Gnor and GLA, with an average $r = 0.20$, as well as plant height ($r = 0.19$). In Canchan, correlations were moderate, with the total number of tubers again standing out ($r = 0.40$), while the texture and color index exhibited weaker relationships, with r values between −0.06 and 0.06; plant height showed a slightly negative correlation ($r = -0.03$). The Shulay variety showed low magnitude correlations, with r values ranging from −0.089 to 0.09; the correlation between yield and the blue band (B) was slightly positive ($r = 0.11$). In the Tahuaqueña variety, a positive trend was again observed between yield and the total number of tubers ($r = 0.34$) as well as the number of affected leaves ($r = 0.11$). The color and texture index exhibited low correlations, with r values between −0.09 and 0.07, while plant height reached $r = 0.06$ (Figure S1).

Although these correlations did not exceed $r = 0.45$, the Pearson analysis disaggregated by phenological stage revealed consistent patterns throughout the crop cycle. The correlations between yield and plant height and total tuber number showed average coefficients of $r = 0.31$ and $r = 0.49$, respectively ($p < 0.001$), across all phenological stages.

Agronomic variables (yield, plant height and total number of tubers) exhibited the strongest correlations with color indices ($r = 0.2-0.6$). Only during the onset of tuberization and tuber bulking stages did the correlations between agronomic variables and texture indices increase, reaching an average of $r = 0.38$. In these same stages, the correlations between texture and color indices became even stronger, with average r values of 0.71 at the onset of tuberization and 0.58 during tuber bulking.

The color indices (VARI, GRVI, MGRVI, CIVE, EXG, GLA, among others) maintained high correlations across all phenological stages ($r > 0.8$ or $r < -0.8$), indicating strong interdependence and high spectral redundancy. Nevertheless, the correlations between the normalized red band index (Rnor) and the color indices tended to decrease toward physiological maturity, reaching $r = -0.09$, without significant differences. Negative correlations close to −1 indicate that certain indices capture the same reflectance variation but in inverse scales (Figure S2).

This analysis made it possible to identify relationship patterns, detect multicollinearity and select the most relevant variables for the yield estimation and variety identification models. Consequently, predictive models of yield were developed according to the phenological stages and the ability of RGB images to distinguish potato varieties was evaluated.

3.4. Modeling Using UAV Image Information for Yield Estimation and Variety Identification in Potato Crops

3.4.1. Yield Modelling

The yield modelling performed using the Random Forest (RF) and Gradient Boosting (GB) models across the different phenological stages, from stolon development to physiological maturity, showed R^2 values ranging from 0.44 to 0.66 for RF and from 0.44 to 0.62 for GB. During the stolon development phase, the RF model exhibited slightly better performance than GB, with a 4% higher R^2 and a 0.10 t ha^{-1} lower RMSE. In the early tuberization phase, the GB model slightly outperformed RF, with a 2% higher R^2 and a 0.05 t ha^{-1} lower RMSE. In the tuber filling phase, the RF model again outperformed GB, with similar differences to those observed during stolon development (4% higher R^2 and −0.10 t ha^{-1} in RMSE). At physiological maturity, both models showed equivalent R^2 and RMSE values, indicating comparable performance in yield prediction. Considering all the evaluated phenological stages together, both models showed similar overall results: RF achieved an average R^2 of 0.54 and an RMSE of 2.72 t ha^{-1}, while GB obtained an average R^2 of 0.52 and an RMSE of 2.75 t ha^{-1} (Table 3).

Table 3. Performance analysis of machine learning models in forecasting crop yield at distinct growth stages for the 2024–2025 period using Leave-One-Out Cross-Validation (CV).

Phase	n	Gradient Boosting			Random Forest			*p*-Value
		R2_CV	RMSE_CV (t ha^{-1})	Rrmse_CV (%)	R2_CV	RMSE_CV (t ha^{-1})	Rrmse_CV (%)	
Stolon development	58	0.62	2.41	23.30	0.66	2.31	22.32	0.0534
Onset of tuber initiation	58	0.53	2.69	26.04	0.51	2.74	26.49	0.4881
Tuber bulking	58	0.49	2.80	27.15	0.53	2.69	26.02	0.2248
Physiological maturity	116	0.45	3.13	30.28	0.45	3.13	30.29	0.0436
Average for potato cultivation		0.52	2.75	26.69	0.54	2.72	26.28	

The dispersion of values around the 1:1 line between the yield estimated by both models and the measured yield is shown in Figure S3. The predicted values ranged from 3 to 17 t ha^{-1}, while the measured values varied between 4 and 16 t ha^{-1}, demonstrating a good correspondence between the two datasets Average R^2 values of 0.64, 0.52, and 0.51 were obtained for earlier stages, whereas physiological maturity presented greater dispersion (R^2 = 0.44), reflecting reduced model accuracy at late developmental stages.

The relative importance of the predictor variables used in both models is shown in Figure 8. During the stolon development phase, the indices Rnor, CIVE, HL and EXG had the greatest impact on the model, with values of 0.14, 0.13 and 0.11, respectively, in RF and 0.24, 0.22 and 0.19 for GB, highlighting the relevance of reflectance in the visible bands associated with early vegetative vigor. At the onset of tuberization, the RF model identified Blue band B (0.14), plant height (0.13) and AL (0.12) as the most influential variables, while GB assigned greater importance to B (0.21), Bnor (0.18) and plant height (0.16), indicating

that canopy structure begins to reflect growth differences. During the tuber filling phase, the variables CON (0.14), plant height (0.13) and COR (0.11) were the most determinant in RF, whereas in GB the most influential variables were MGRVI (0.23), plant height (0.19) and HL (0.17). At physiological maturity, both models agreed on the relevance of plant height, with an average importance of 0.14 in RF and 0.22 in GB. This was followed by the indices HL and CIVE, with values between 0.09 and 0.11, while the color and texture indices showed a lower contribution, with values below 0.05.

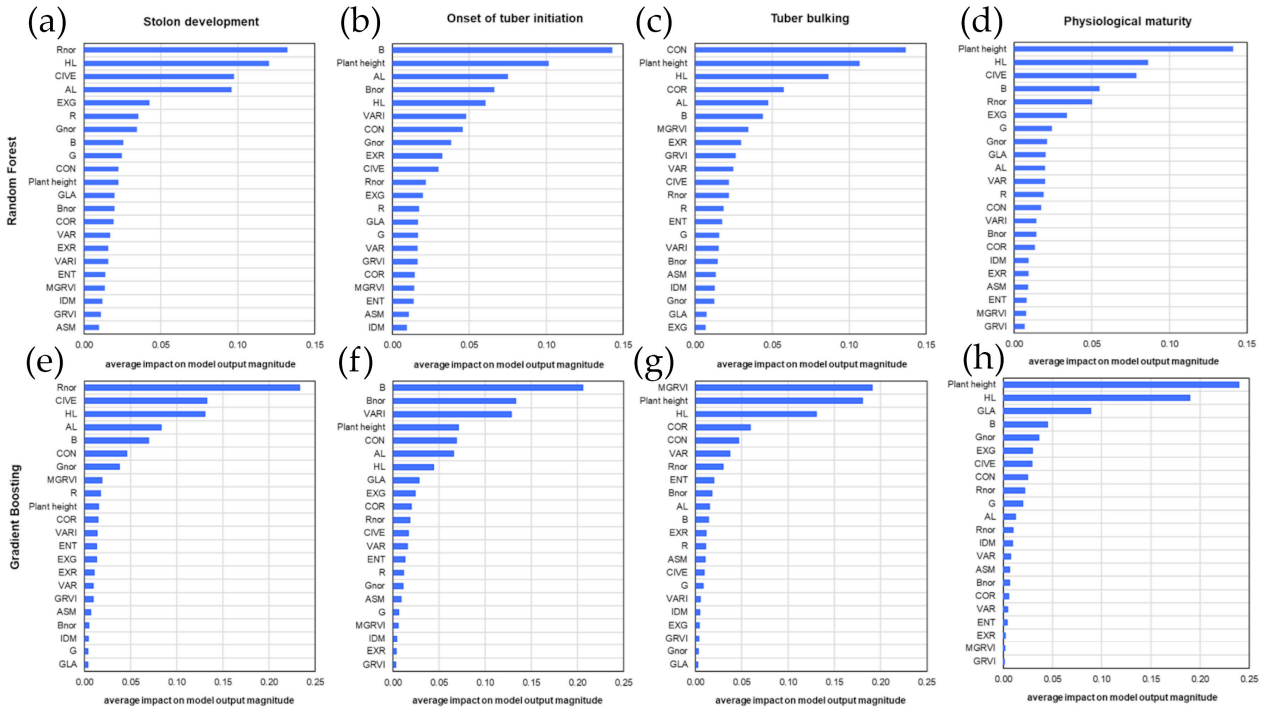

Figure 8. Average impact of feature importance on yield prediction in phases of (**a**,**e**) Stolon development, (**b**,**f**) Onset of tuber initiation, (**c**,**g**) Tuber bulking and (**d**,**h**) Physiological maturity of potato cultivation using Random Forest and Gradient Boosting models.

3.4.2. Modeling of Variety Identification

The performance of different architectures and classification strategies for identifying INIA potato varieties (Bicentenario, Canchan, Shulay and Tahuaqueña) from RGB images was evaluated. Convolutional neural network (CNN) models and the Random Forest model (trained with embeddings) showed strong performance, achieving CV F1-macro values above 0.60. In contrast, the remaining models obtained values between 0.40 and 0.57, indicating more limited classification accuracy (Table 4).

Table 4. Comparative performance of machine learning and deep learning models in the identification of potato varieties from UAV-RGB images.

Modelo	CV F1-Macro	Accuracy (%)
CNN	0.69	72
Random Forest	0.66	73
SVM (RBF)	0.55	62
Decision Tree	0.57	61
Regresión Logística	0.51	55
KNN	0.40	42

The CNN achieved an F1-macro of 0.69. Among the varieties, Bicentenario achieved the best metrics (recall = 0.91; F1-score = 0.80), indicating high recognition accuracy. Shulay

also performed well (F1 = 0.76), while Canchan (F1 = 0.61) and Tahuaqueña (F1 = 0.58) showed lower classification precision.

The global performance of the three CNN configurations evaluated is summarized in Table 5, where the optimized CNN achieved the highest accuracy (72%) and macro-F1 (0.69). Detailed per-class precision, recall, F1-score and sample support for the optimized CNN are reported in Table 6. The confusion matrix presented in Table 7 reveals systematic misclassifications between Canchan and Tahuaqueña, confirming that class imbalance negatively affected the discrimination of underrepresented varieties, particularly Tahuaqueña.

Table 5. Global performance comparison of the three CNN configurations evaluated for potato variety identification. The optimized CNN achieved the highest accuracy and macro F1 score.

Modelo	Accuracy (%)	Macro F1	Best Class (F1)	Worst Class (F)
Traditional CNN (without balancing)	64	0.61	Bicentenario (0.82)	Canchan (0.47)
Traditional CNN (with selective balancing)	66	0.62	Bicentenario (0.84)	Tahuaqueña (0.41
Optimized CNN	72	0.69	Bicentenario (0.80)	Tahuaqueña (0.58)

Table 6. Per- class performance metrics for the optimized CNN model.

Class	Precision	Recall	F1-Score	Support
Bicentenario	0.71	0.91	0.80	90
Canchan	0.71	0.53	0.61	60
Shulay	0.77	0.75	0.76	106
Tahuanqueña	078	0.46	0.58	56

Table 7. Confusion matrix of the optimized CNN model.

Actual/Predicted	Bicentenario	Canchan	Shulay	Tahuaqueña
Bicentenario	82	2	4	2
Canchan	8	32	10	10
Shulay	8	4	80	14
Tahuaqueña	6	11	13	26

Comparing the five models trained with embeddings for variety identification, Random Forest achieved the best overall performance, with a cross-validated F1-macro of 0.66 and ROC AUC of 0.89, demonstrating strong class separation and generalization capability. It was followed by SVM (55%) and Decision Tree (57%). Logistic Regression performed moderately (CV F1-macro = 0.51), while KNN obtained the lowest results (<0.40) (Figure 9).

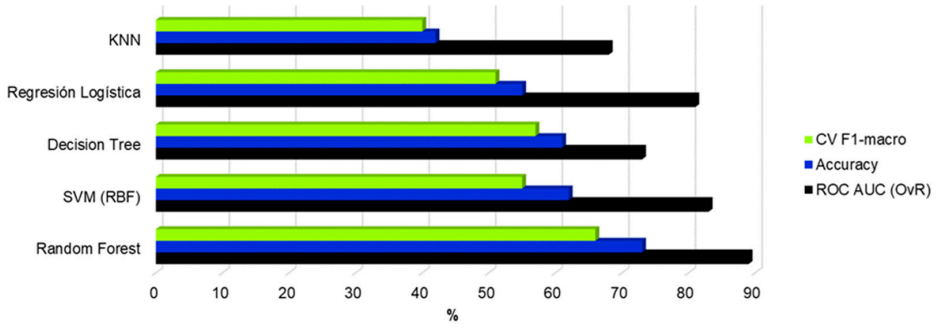

Figure 9. Comparison of models that used EfficientNetB0 embeddings for the identification of potato varieties.

4. Discussion

4.1. Yield Estimation

The results clearly demonstrate significant differences in the agronomic parameters of four potato varieties across distinct phenological stages under uniform cultivation conditions. The Tahuaqueña variety consistently exhibited greater vegetative growth at all stages compared to the Bicentenario variety. The average stem height was 57.61 cm, exceeding the 38 cm average reported for potato clones in Huancayo department, another Andean Peruvian locality, under different treatments [40].

When analyzing the correlations by variety, very low values ($r < 0.1$) were observed between yield and color and textural indices, indicating a weak or nonexistent dependency on visual canopy characteristics. This may be attributed to the structural uniformity of the canopy or lower foliar variability among varieties, which reduces spectral sensitivity and the observable phenotypic range. This finding is consistent with de [102], who reported LAI saturation when the canopy exceeded 3 m^2 m^{-2}, reflecting a loss of sensitivity in uniform canopies. Similarly, ref. [103] found that the predictive capacity of UAV-derived indices for yield remained high (R^2 = 0.76–0.93) only when there was variation across growth phases or stages, whereas accuracy declined significantly when canopy variability was low.

Nonetheless, the positive correlations maintained between yield, number of tubers, plant height and greenness indices (EXG, Gnor) suggest that a more vigorous and photosynthetically active canopy translates into greater yield potential. This aligns with [104], who demonstrated that differences in the rate of leaf appearance (phyllochron) and leaf expansion determine the photosynthetic capacity of the canopy and, consequently, the proportion of large tubers.

When observations were grouped by phenological stage, the correlations between spectral indices and yield increased significantly (r = 0.45–0.60), consistent with the findings of [96], who observed increases of 43–48% in the photosynthetic rate and leaf area index (LAI) during tuber filling, associated with greater radiation interception. This pattern suggests that during active growth phases, spectral indices more accurately capture canopy dynamics and photosynthetic efficiency, as they are closely related to plant vigor and leaf expansion.

In contrast, during the later stages of the crop (physiological maturity), correlations decreased as senescence progressed and canopy heterogeneity increased. This aligns with the findings of [105], who reported reductions of 37% in chlorophyll, 46% in yield, and a drop in LAI from 5.8 to 2.4 under severe water stress. Similarly, ref. [106] demonstrated that the predictive capacity of spectral indices diminishes towards the end of the cycle when stomatal conductance and photosynthetic rate are reduced by up to 96–98% compared to the control. In order to explore better this aspect, two predictive modeling approaches were conducted using Random Forest and Gradient Boosting, aiming to develop and evaluate a model for predicting agricultural yield from RGB images obtained with UAVs by phenological phase.

In the predictive analysis, the results show that the Random Forest (RF) algorithm exhibited the best overall performance in estimating yield across the four phenological phases compared to Gradient Boosting (GB). Its superior predictive capacity during the stolon development phase (R^2 = 0.66, RMSE = 2.31) can be attributed to its capacity to capture nonlinear relationships between spectral and agronomic variables while minimizing overfitting through tree aggregation [107]. These findings are consistent with [108], who obtained $R^2 \approx 0.52$ using textural and vegetation indices derived from UAV multispectral imagery during the flowering stages of rice cultivation. Additionally, ref. [109] in Egypt achieved R^2 = 0.80 for total tuber yield by combining RGB color indices and thermal in-

formation using ANFIS-GA (hybrid model of artificial intelligence), suggesting that the inclusion of thermal imagery could further enhance yield prediction accuracy.

A similar trend was observed in maize cultivation under northern U.S. climatic conditions, where R^2 increased at advanced crop stages but RMSE decreased in the intermediate phase and remained stable until maturity [95]. On the other hand, ref. [110] reported yields ranging from 30 to 80 t ha^{-1} in Spain, achieving RMSE = 8.76 t ha^{-1} and R^2 = 0.89 using Random Forest applied to Sentinel satellite imagery. This high coefficient of determination may be linked to the broader environmental variability of the crop and the larger observational scale used. These findings indicate that the relationship between sensor resolution and crop phenology strongly influences the predictive capacity of RGB images, whose moderate performance and cost-effectiveness can still be effectively leveraged [47,48]. Meanwhile, integrating multispectral and thermal bands generally enhances precision [108,109].

4.2. Identification of Potato Varieties

The enhanced CNN architecture achieved an overall accuracy of 72% and a macro F1-score of 0.69, while the Random Forest model using EfficientNetB0 embeddings achieved comparable accuracy (73.4%) and a macro F1-score of 0.72 [111]. These results confirm the feasibility of employing RGB imagery for varietal discrimination despite the sensor's limited spectral resolution. Comparatively, ref. [112] applied YOLOv8 and Vision Transformer models to multispectral imagery, achieving accuracies above 85%. However, these approaches demand greater computational resources and advanced sensors, which limit their applicability in rural field contexts. Therefore, the present findings are noteworthy and reproducible under field conditions using economically accessible equipment [113].

Regarding class-specific performance, the improved CNN exhibited heterogeneous accuracy among varieties. The Bicentenario variety achieved the highest performance (recall = 0.91; F1 = 0.80), indicating that the model effectively recognized most of its instances. Similarly, Shulay achieved F1 = 0.76, suggesting that both varieties possess distinctive morphological traits that facilitate discrimination by the network [100,114]. In contrast, Canchan (F1 = 0.61) and particularly Tahuaqueña (F1 = 0.58) showed lower classification accuracy [95]. This outcome may be explained by (1) the smaller number of training samples for these varieties, which limits generalization, and (2) their high visual similarity, which increases confusion in the CNN's feature space.

The use of pre-trained EfficientNetB0 embeddings proved to be an efficient, low-cost alternative compared to training CNNs from scratch. This strategy allowed leveraging high-level representations generated by deep networks without the need for large volumes of data, drastically reducing training time and the risk of overfitting as shown. Random Forest is the model with the best overall performance with a CV macro F1 = 0.66 and a ROC AUC of 0.89, demonstrating consistent class separation and good generalization capacity. Similar results were reported by [114], where the classification of two potato cultivars using hyperspectral images in cultivar recognition obtained similar metrics ROC AUC = 0.87, CV F1 with biased values from 0.63 to 0.67 and biased by plant CV F1 = 0.77. Practically, the achieved accuracy (≈72%) positions this methodology as one of the first methodological references for varietal identification of potatoes in the southern highlands of Peru. Its main contribution lies in validating a low-cost, reproducible and scientifically solid approach that can be integrated into genetic improvement and phenotypic monitoring programs [95,100].

For future improvement, it is recommended to expand the dataset through data augmentation, explore deeper architectures (EfficientNetB3, ConvNeXt, Vision Transformer), and integrate RGB imagery with complementary variables such as growth and chlorophyll data. Those strategies could improve accuracy by 10–15%, achieving re-

sults comparable to multispectral sensors while maintaining accessibility for small- and medium-scale producers [111,115].

5. Conclusions

This study demonstrates that the integration of UAV-acquired RGB imagery with machine learning approaches and conventional agronomic measurements provides a feasible and cost-effective framework for potato yield estimation and varietal identification under high Andean conditions in southern Peru. Clear genotypic differences among the evaluated varieties highlight the relevance of combining field-based agronomic traits with canopy-level information derived from UAV data.

For yield prediction, Random Forest models showed greater robustness than alternative approaches, particularly during the stolon development stage, emphasizing the importance of phenological timing in UAV-based assessments. Prediction accuracy decreased during later stages due to foliar senescence, underscoring inherent limitations of RGB reflectance when the canopy structure and physiological status change.

Varietal identification using UAV-RGB imagery achieved consistent and acceptable performance through both convolutional neural networks and classical classifiers trained on deep learning embeddings. These results confirm that RGB-based methods can capture relevant phenotypic differences among potato varieties, even in resource-limited settings.

Nevertheless, several limitations should be acknowledged. The low correlation between RGB-derived indices and yield ($r < 0.3$) reflects the inherent constraints of visible reflectance data for capturing subsurface biomass, especially during senescence. The evaluation of only four varieties limits the generalizability of the models, and the absence of additional spectral information restricts the detection of key physiological traits. Moreover, varietal classification accuracy may decrease when canopy structures are highly similar or when phenological stages are not synchronized.

Future research should expand the number and diversity of evaluated genotypes, incorporate multispectral or thermal sensors, and increase the temporal density of UAV acquisitions across phenological stages. Integrating soil, climatic, and management data would further improve model robustness and enable a deeper understanding of genotype $\times$ environment interactions in high Andean potato systems.

Supplementary Materials: The following supporting information can be downloaded at: https://www.mdpi.com/article/10.3390/agriengineering8020065/s1. Figure S1. Pearson correlation coefficient (r) between yield with agronomic variables, color and textural index for the four potato varieties: (a) Bicentenario, (b) Canchan, (c) Shulay and (d) Tahuaqueña. Figure S2. Pearson correlation map between agronomic variables, color and texture index by phenological stage: (a) stolon development, (b) onset of tuber initiation, (c) tuber bulking and (d) physiological maturity; Figure S3. Predicted versus measured yield for Gradient Boosting and Random Forest across the four growth phases of potato crops during the 2024–2025 period.

Author Contributions: Conceptualization, M.T. and M.G.; methodology, M.T. and M.G.; software, O.P.; validation, R.B., M.T. and P.C.; formal analysis, M.T., R.G., R.B. and W.M.; resources, R.G.; J.P., J.A. and P.C.; data curation, W.M., J.P., M.T. and M.G.; writing—original draft preparation M.T., D.M. and M.G.; writing—review and editing, D.M.; supervision, D.M.; project administration, O.P. and J.A.; funding acquisition, O.P. All authors have read and agreed to the published version of the manuscript.

Funding: The study titled 'Varietal Identification and Yield Estimation in Potatoes Using UAV-RGB Imagery in the Southern Highlands of Peru' was funded by investment project 2361771: 'Improvement of the Availability, Access, and Use of Quality Seeds of Potato, Amylaceous maize, Grain Legumes, and Cereals in the Regions of Junín, Ayacucho, Cusco, and Puno (4 Departments),' supported by the National Institute of Agrarian Innovation (INIA), Peru.

Institutional Review Board Statement: Not applicable.

Informed Consent Statement: Not applicable.

Data Availability Statement: The original contributions presented in the study are included in the article; any additional inquiries can be directed to the corresponding author.

Conflicts of Interest: The authors declare no conflicts of interest.

Abbreviations

The following abbreviations are used in this manuscript:

INIA	Instituto Nacional de Innovación Agraria
RGB	Red-Green-Blue
UAV	Unmanned Aerial Vehicle
CNN	Convolutional Neural Network
HTP	High Throughput Phenotyping
GLCM	Gray Level Co-occurrence Matrix
RTK	Real-Time Kinematic
RF	Random Forest
GB	Gradient Boosting
KNN	K-Nearest Neighbors
ROC	Receiver Operating Characteristic
SVM	Support Vector Machine
AUC	Area Under the Curve
RMSE	The root mean square error
MAE	The mean absolute error

References

1. Pandey, J.; Gautam, S.; Scheuring, D.C.; Koym, J.W.; Vales, M.I. Variation and genetic basis of mineral content in potato tubers and prospects for genomic selection. *Front. Plant Sci.* **2023**, *14*, 1301297. [CrossRef]
2. Spooner, D.M.; McLean, K.; Ramsay, G.; Waugh, R.; Bryan, G.J. A single domestication for potato revealed by AFLP genotyping. *Proc. Natl. Acad. Sci. USA* **2005**, *102*, 14694–14699. [CrossRef] [PubMed]
3. Xaba, S.; Bello, Z.; Rapiya, M.; Ngobese, N.Z. Sustainable nutrient management strategies for enhancing potato production: The role of cover crops—A systematic review. *Horticulturae* **2025**, *11*, 1051. [CrossRef]
4. Larkin, R.P. Potato cropping system and variety impacts on soil properties, soilborne diseases, and tuber yield in a long-term field trial. *Agronomy* **2024**, *14*, 2852. [CrossRef]
5. Hu, X.; Jiang, H.; Liu, Z.; Gao, M.; Liu, G.; Tian, S.; Zeng, F. The global potato-processing industry: A review of production, products, quality and sustainability. *Foods* **2025**, *14*, 1758. [CrossRef] [PubMed]
6. MIDAGRI. *El Perú es el Primer Productor de Papa en América Latina y el Sustento de Más de 700 Mil Familias*; Ministerio de Desarrollo Agrario y Riego: Lima, Perú, 2024.
7. Perez, E.; Rafael-Rutte, R.; Osorio, G. Estrés hídrico en el crecimiento y rendimiento de cultivares comerciales de papa (*Solanum tuberosum* L.) en la región centro del Perú. *Rev. Investig. Altoandinas* **2024**, *26*, 46–55. [CrossRef]
8. Pinedo-Taco, R.; Olivas Alvarado, T. Niveles de absorción de NPK y rendimiento del cultivo de papa en función a la dosis y método de fertilización fraccionada. *Idesia* **2023**, *41*, 21–30. [CrossRef]
9. Hijmans, R.J. The effect of climate change on global potato production. *Am. J. Potato Res.* **2003**, *80*, 271–279. [CrossRef]
10. Zárate Malpica, A.H.; Miranda Zambrano, G.A. Impacto del cambio climático en la seguridad alimentaria en zonas campesinas vulnerables de los Andes del Perú. *Rev. Mex. Cienc. Agric.* **2017**, *7*, 71–82. [CrossRef]
11. Ibrahim Ibrahim, S.; Naawe, E.K.; Çalışkan, M.E. Effect of drought stress on morphological and yield characteristics of potato (*Solanum tuberosum* L.) breeding lines. *Potato Res.* **2024**, *67*, 529–543. [CrossRef]
12. González-Jiménez, J.; Andersson, B.; Wiik, L.; Zhan, J. Modelling potato yield losses caused by *Phytophthora infestans*: Aspects of disease growth rate, infection time and temperature under climate change. *Field Crops Res.* **2023**, *299*, 108977. [CrossRef]
13. Asakaviciute, R.; Zelya, A.; Andriychuk, T.; Razukas, A. Evaluation of Potato Varieties for Yield, Quality, and Late Blight Resistance. *Life* **2025**, *15*, 1378. [CrossRef]
14. Meno, L.; Abuley, I.; Seijo, M.C.; Escuredo, O. Management Strategies for Early Blight in Potatoes: Assessment of the TOMCAST Model, Including the Aerobiological Risk Level and Critical Phenological Period. *Agriculture* **2024**, *14*, 1414. [CrossRef]

15. Rivas, S.; Fincheira, P.; González, F.; Santander, C.; Meier, S.; Santos, C.; Contreras, B.; Ruiz, A. Assessment of the Photosynthetic Response of Potato Plants Inoculated with *Rhizoctonia solani* and Treated with Flesh-Colored Potato Extracts Nanoencapsulated with Solid Lipid Nanoparticles. *Plants* **2025**, *14*, 156. [CrossRef] [PubMed]
16. Sandaña, P.; Lizana, C.X.; Pinochet, D.; Santana, J.; Carrera, R. The Ecophysiological Determinants of Tuber Yield in Response to Potato Genotype and Nitrogen Availability. *Agronomy* **2023**, *13*, 1971. [CrossRef]
17. Wen, L.; Meng, M.; Liu, K.; Zhang, Q.; Zhang, T.; Chen, Y.; Liang, H. Effect of Photoperiod on Dry Matter Accumulation and Partitioning in Potato. *Agriculture* **2024**, *14*, 1156. [CrossRef]
18. Shen, C.; Yang, W.; Kang, Y.; Qin, S.; Zhang, W.; Liu, Y.; Qian, S.; Han, Y. Effect of Alkaline Salt Stress on Photosynthetic Activities of Potato Plants (*Solanum tuberosum* L.). *Plants* **2025**, *14*, 2979. [CrossRef]
19. Nasir, M.W.; Toth, Z. Effect of Drought Stress on Potato Production: A Review. *Agronomy* **2022**, *12*, 635. [CrossRef]
20. Instituto Nacional de Innovación Agraria (INIA); Centro Internacional de la Papa (CIP). *Catálogo de Nuevas Variedades de Papa: Sabores y Colores Para el Gusto Peruano*; Red Latin Papa: Lima, Perú, 2012. [CrossRef]
21. Devaux, A.; Ordinola, M.; Suarez, V.; Hareau, G. Situación Actual y Perspectivas del Procesamiento de Papa en la Zona Andina, Implicancias Para el Mejoramiento Genético y la Selección de Variedades. International Potato Center (CIP). 2024. Available online: https://cgspace.cgiar.org/handle/10568/168128 (accessed on 15 December 2025).
22. Pinedo-Taco, R.; Olivas-Alvarado, T.; Rodríguez-Soto, G.; Castro-Cepero, V. Effect of nitrogen and phosphorus fertilization sources on the potato crop yield (*Solanum tuberosum* L.). *Rev. Fac. Nac. Agron. Medellín* **2020**, *73*, 9255–9261. [CrossRef]
23. Cabrera, H.; Otiniano, R.; Pando, R.; Garcia, H.S.; Rodriguez, W.H.; Pérez, J.M.; Gastelo, M. INIA 333–Chugay: A new potato variety resilient to climate change for the family farming system with tolerance to frost, resistant to late blight and high quality for fresh consumption. *Am. J. Potato Res.* **2025**, *102*, 119–128. [CrossRef]
24. Ayankojo, I.T.; Thorp, K.R.; Thompson, A.L. Advances in the application of small unoccupied aircraft systems (sUAS) for high-throughput plant phenotyping. *Remote Sens.* **2023**, *15*, 2623. [CrossRef]
25. Zahra, S.; Ruiz, H.; Jung, J.; Adams, T. UAV-based phenotyping: A non-destructive approach to studying wheat growth patterns for crop improvement and breeding programs. *Remote Sens.* **2024**, *16*, 3710. [CrossRef]
26. Yuan, J.; Zhang, Y.; Zheng, Z.; Yao, W.; Wang, W.; Guo, L. Grain crop yield prediction using machine learning based on UAV remote sensing: A systematic literature review. *Drones* **2024**, *8*, 559. [CrossRef]
27. Gerakari, M.; Katsileros, A.; Kleftogianni, K.; Tani, E.; Bebeli, P.J.; Papasotiropoulos, V. Breeding of solanaceous crops using AI: Machine learning and deep learning approaches—A critical review. *Agronomy* **2025**, *15*, 757. [CrossRef]
28. Michel, S.; Löschenberger, F.; Ametz, C.; Bistrich, H.; Bürstmayr, H. Can we teach machines to select like a plant breeder? A recommender system approach to support early generation selection decisions based on breeders' preferences. *Crops* **2025**, *5*, 31. [CrossRef]
29. Victor, B.; Nibali, A.; Newman, S.J.; Coram, T.; Pinto, F.; Reynolds, M.; Furbank, R.T.; He, Z. High-throughput plot-level quantitative phenotyping using convolutional neural networks on very high-resolution satellite images. *Remote Sens.* **2024**, *16*, 282. [CrossRef]
30. Phang, S.K.; Chiang, T.H.A.; Happonen, A.; Chang, M.M.L. From satellite to UAV-based remote sensing: A review on precision agriculture. *IEEE Access* **2023**, *11*, 127057–127076. [CrossRef]
31. Chakhvashvili, E.; Machwitz, M.; Antala, M.; Rozenstein, O.; Prikaziuk, E.; Schlerf, M.; Naethe, P.; Wan, Q.; Komárek, J.; Klouek, T.; et al. Crop stress detection from UAVs: Best practices and lessons learned for exploiting sensor synergies. *Precis. Agric.* **2024**, *25*, 2614–2642. [CrossRef]
32. Abbas, A.; Zhang, Z.; Zheng, H.; Alami, M.M.; Alrefaei, A.F.; Abbas, Q.; Naqvi, S.A.H.; Rao, M.J.; Mosa, W.F.A.; Abbas, Q.; et al. Drones in plant disease assessment, efficient monitoring, and detection: A way forward to smart agriculture. *Agronomy* **2023**, *13*, 1524. [CrossRef]
33. Gao, M.; Yang, F.; Wei, H.; Liu, X. Automatic monitoring of maize seedling growth using unmanned aerial vehicle-based RGB imagery. *Remote Sens.* **2023**, *15*, 3671. [CrossRef]
34. Goswami, A.; Khati, U.; Goyal, I.; Sabir, A.; Jain, S. Automated stock volume estimation using UAV-RGB imagery. *Sensors* **2024**, *24*, 7559. [CrossRef] [PubMed]
35. Lee, C.-H.; Chen, K.-Y.; Liu, L.D. Effect of texture feature distribution on agriculture field type classification with multitemporal UAV RGB images. *Remote Sens.* **2024**, *16*, 1221. [CrossRef]
36. Wu, J.; Zheng, D.; Wu, Z.; Song, H.; Zhang, X. Prediction of buckwheat maturity in UAV-RGB images based on recursive feature elimination cross-validation: A case study in Jinzhong, Northern China. *Plants* **2022**, *11*, 3257. [CrossRef]
37. Ye, Y.; Jin, L.; Bian, C.; Liu, J.; Guo, H. Monitoring and optimization of potato growth dynamics under different nitrogen forms and rates using UAV RGB imagery. *Agronomy* **2024**, *14*, 2257. [CrossRef]
38. Li, B.; Xu, X.; Han, J.; Zhang, L.; Bian, C.; Jin, L.; Liu, J. The estimation of crop emergence in potatoes by UAV RGB imagery. *Plant Methods* **2019**, *15*, 15. [CrossRef]

39. Yin, H.; Yang, H.; Hu, Y.; Li, F.; Yu, K. Drone RGB imagery color and texture information have varied importance in predicting potato aboveground biomass in different growth stages. *Potato Res.* **2025**, *68*, 2971–2996. [CrossRef]
40. Ccopi, D.; Ortega, K.; Castañeda, I.; Rios, C.; Enriquez, L.; Patricio, S.; Ore, Z.; Casanova, D.; Agurto, A.; Zuñiga, N.; et al. Using UAV images and phenotypic traits to predict potato morphology and yield in Peru. *Agriculture* **2024**, *14*, 1876. [CrossRef]
41. Kozhekin, M.V.; Genaev, M.A.; Komyshev, E.G.; Zavyalov, Z.A.; Afonnikov, D.A. Plant detection in RGB images from unmanned aerial vehicles using segmentation by deep learning and the impact of model accuracy on downstream analysis. *J. Imaging* **2025**, *11*, 28. [CrossRef]
42. Tariku, G.; Ghiglieno, I.; Simonetto, A.; Gentilin, F.; Armiraglio, S.; Gilioli, G.; Serina, I. Advanced image preprocessing and integrated modeling for UAV plant image classification. *Drones* **2024**, *8*, 645. [CrossRef]
43. Zheng, Z.; Yuan, J.; Yao, W.; Yao, H.; Liu, Q.; Guo, L. Crop classification from drone imagery based on lightweight semantic segmentation methods. *Remote Sens.* **2024**, *16*, 4099. [CrossRef]
44. Yu, F.; Zhang, Q.; Xiao, J.; Ma, Y.; Wang, M.; Luan, R.; Liu, X.; Ping, Y.; Nie, Y.; Tao, Z.; et al. Progress in the application of CNN-based image classification and recognition in whole crop growth cycles. *Remote Sens.* **2023**, *15*, 2988. [CrossRef]
45. Khan, M.N.; Tan, Y.; He, L.; Dong, W.; Dong, S. From air to space: A comprehensive approach to optimizing aboveground biomass estimation on UAV-based datasets. *Forests* **2025**, *16*, 214. [CrossRef]
46. Sun, C.; Zhou, J.; Ma, Y.; Xu, Y.; Pan, B.; Zhang, Z. A review of remote sensing for potato traits characterization in precision agriculture. *Front. Plant Sci.* **2022**, *13*, 871859. [CrossRef]
47. Kior, A.; Yudina, L.; Zolin, Y.; Sukhov, V.; Sukhova, E. RGB imaging as a tool for remote sensing of characteristics of terrestrial plants: A review. *Plants* **2024**, *13*, 1262. [CrossRef]
48. Stuart, M.B.; McGonigle, A.J.S.; Davies, M.; Hobbs, M.J.; Boone, N.A.; Stanger, L.R.; Zhu, C.; Pering, T.D.; Willmott, J.R. Low-cost hyperspectral imaging with a smartphone. *J. Imaging* **2021**, *7*, 136. [CrossRef]
49. Neina, D. Role of soil pH in plant nutrition and soil remediation. *Appl. Environ. Soil Sci.* **2019**, *2019*, 5794869. [CrossRef]
50. Molua, C.O. Investigating the influence of soil electrical conductivity on crop yield for precision agriculture advancements. *Int. J. Agric. Anim. Prod.* **2021**, *12*, 23–34. [CrossRef]
51. King, A.E.; Ali, G.A.; Gillespie, A.W.; Wagner-Riddle, C. Soil organic matter as catalyst of crop resource capture. *Front. Environ. Sci.* **2020**, *8*, 50. [CrossRef]
52. Chatraei Azizabadi, E.; El-Shetehy, M.; Cheng, X.; Youssef, A.; Badreldin, N. In-season potato nitrogen prediction using multispectral drone data and machine learning. *Remote Sens.* **2025**, *17*, 1860. [CrossRef]
53. Muindi, E.M. Understanding soil phosphorus. *Int. J. Plant Soil Sci.* **2019**, *31*, 1–18. [CrossRef]
54. Xu, X.; Du, X.; Wang, F.; Sha, J.; Chen, Q.; Tian, G.; Zhu, Z.; Ge, S.; Jiang, Y. Effects of potassium levels on plant growth, accumulation and distribution of carbon, and nitrate metabolism in apple dwarf rootstock seedlings. *Front. Plant Sci.* **2020**, *11*, 904. [CrossRef] [PubMed]
55. Ierna, A.; Distefano, M. Crop Nutrition and Soil Fertility Management in Organic Potato Production Systems. *Horticulturae* **2024**, *10*, 886. [CrossRef]
56. Burton, D.L.; Zebarth, B.J.; Gillam, K.M.; MacLeod, J.A. Effect of Split Application of Fertilizer Nitrogen on N_2O Emissions from Potatoes. *Can. J. Soil Sci.* **2008**, *88*, 229–239. [CrossRef]
57. Kiba, D.; Wakenva, J.; Atinkpah, B.; Foca, D.; Salifou, P.; Guèdègbé, G.; Kodjovi-Adjé, C. Synthetic Fertilizer Application Coupled with Bioslurry Optimizes Potato (*Solanum tuberosum*) Growth and Yield. *Agronomy* **2023**, *13*, 2162. [CrossRef]
58. Torabian, S.; Farhangi-Abriz, S.; Qin, R.; Noulas, C.; Sathuvalli, V.; Charlton, B.; Loka, D. Potassium: A Vital Macronutrient in Potato Production—A Review. *Agronomy* **2021**, *11*, 543. [CrossRef]
59. Rakibuzzaman, M.; Akand, M.H.; Siddika, M.; Uddin, A.F.M.J. Impact of *Trichoderma* application as bio-stimulator on disease suppression, growth and yield of potato. *J. Biosci. Agric. Res.* **2021**, *27*, 2252–2257. [CrossRef]
60. Sales, L.R.; Rigobelo, E.C. The role of *Bacillus* sp. in reducing chemical inputs for sustainable crop production. *Agronomy* **2024**, *14*, 2723. [CrossRef]
61. Wickham, H.; François, R.; Henry, L.; Müller, K. *Dplyr: A Grammar of Data Manipulation*, version 1.1.4; R Package for Data Manipulation; Posit Software, PBC: East Greenwich, RI, USA, 2023. Available online: https://CRAN.R-project.org/package=dplyr (accessed on 15 December 2025).
62. Mair, P.; Wilcox, R. *WRS2: Robust Statistical Methods*, version 1.14; R Package for Data Manipulation; Posit Software, PBC: East Greenwich, RI, USA, 2023. Available online: https://CRAN.R-project.org/package=WRS2 (accessed on 15 December 2025).
63. Zhicheng, D.; Feng, H. *RHSD: Ryan–Holm Step-Down Bonferroni or Sidak*, version 0.2.0; R Package for Data Manipulation; Posit Software, PBC: East Greenwich, RI, USA, 2022. Available online: https://cran.r-project.org/web/packages/RHSDB/index.html (accessed on 15 December 2025).
64. Shammi, S.A.; Huang, Y.; Feng, G.; Tewolde, H.; Zhang, X.; Jenkins, J.; Shankle, M. Application of UAV multispectral imaging to monitor soybean growth with yield prediction through machine learning. *Agronomy* **2024**, *14*, 672. [CrossRef]

65. Wang, L.; Chen, S.; Peng, Z.; Huang, J.; Wang, C.; Jiang, H.; Zheng, Q.; Li, D. Phenology effects on physically based estimation of paddy rice canopy traits from UAV hyperspectral imagery. *Remote Sens.* **2021**, *13*, 1792. [CrossRef]
66. Kleinsmann, J.; Verbesselt, J.; Kooistra, L. Monitoring individual tree phenology in a multi-species forest using high-resolution UAV images. *Remote Sens.* **2023**, *15*, 3599. [CrossRef]
67. Gao, F.; Anderson, M.; Houborg, R. Impacts of spatial and temporal resolution on remotely sensed corn and soybean emergence detection. *Remote Sens.* **2024**, *16*, 4145. [CrossRef]
68. Maes, W.H. Practical guidelines for performing UAV mapping flights with snapshot sensors. *Remote Sens.* **2025**, *17*, 606. [CrossRef]
69. Bendig, J.; Yu, K.; Aasen, H.; Bolten, A.; Bennertz, S.; Broscheit, J.; Gnyp, M.L.; Bareth, G. Combining UAV-based plant height from crop surface models, visible, and near-infrared vegetation indices for biomass monitoring in barley. *Int. J. Appl. Earth Obs. Geoinf.* **2015**, *39*, 79–87. [CrossRef]
70. Gitelson, A.A.; Merzlyak, M.N.; Chivkunova, O.B. Novel algorithms for remote estimation of vegetation fraction. *Remote Sens. Environ.* **2002**, *80*, 76–87. [CrossRef]
71. Jin, X.; Liu, S.; Baret, F.; Hemerlé, M.; Comar, A. Estimates of plant density of wheat crops at emergence from very low altitude UAV imagery. *Remote Sens. Environ.* **2017**, *198*, 105–114. [CrossRef]
72. Biswal, S.; Pathak, N.; Chatterjee, C.; Mailapalli, D.R. Estimation of aboveground biomass from spectral and textural characteristics of paddy crop using UAV-multispectral images and machine learning techniques. *Geocarto Int.* **2024**, *39*, 2364725. [CrossRef]
73. Haralick, R.M.; Dinstein, I.; Shanmugam, K. Textural features for image classification. *IEEE Trans. Syst. Man Cybern.* **1973**, *SMC-3*, 610–621. [CrossRef]
74. Antoniol, G.; Basco, C.; Ceccarelli, M.; Markus, M.; Moritz, L. *r.texture*—Generate Images with Textural Features from a Raster Map. GRASS GIS Manual. 2025. Available online: https://grass.osgeo.org/grass-stable/manuals/r.texture.html (accessed on 25 May 2025).
75. Tsallis, C. Entropic nonextensivity: A possible measure of complexity. *Chaos Solitons Fractals* **2002**, *13*, 371–391. [CrossRef]
76. Xu, M.; Niu, L.; Wang, X.; Zhang, Z. Evolution of farmland landscape fragmentation and its driving factors in the Beijing–Tianjin–Hebei region. *J. Clean. Prod.* **2023**, *418*, 138031. [CrossRef]
77. McGarigal, K.; Marks, B.J. *FRAGSTATS: Spatial Pattern Analysis Program for Quantifying Landscape Structure (PNW-GTR-351)*; U.S. Department of Agriculture, Forest Service, Pacific Northwest Research Station: Portland, OR, USA, 1995. [CrossRef]
78. Yao, Y.; Cheng, T.; Sun, Z.; Li, L.; Chen, D.; Chen, Z.; Wei, J.; Guan, Q. VecLI: A framework for calculating vector landscape indices considering landscape fragmentation. *Environ. Model. Softw.* **2022**, *149*, 105325. [CrossRef]
79. Bettinger, P.; Bradshaw, G.A.; Weaver, G.W. Effects of geographic information system vector–raster–vector data conversion on landscape indices. *Can. J. For. Res.* **1996**, *26*, 1416–1425. [CrossRef]
80. Wade, T.G.; Wickham, J.D.; Nash, M.S.; Neale, A.C.; Riitters, K.H.; Jones, K.B. A comparison of vector and raster GIS methods for calculating landscape metrics used in environmental assessments. *Photogramm. Eng. Remote Sens.* **2003**, *69*, 1399–1405. [CrossRef]
81. Saura, S.; Torné, J. Conefor Sensinode 2.2: A software package for quantifying the importance of habitat patches for landscape connectivity. *Environ. Model. Softw.* **2009**, *24*, 135–139. [CrossRef]
82. Xu, T.; Wang, F.; Shi, Z.; Miao, Y. Multi-scale monitoring of rice aboveground biomass by combining spectral and textural information from UAV hyperspectral images. *Int. J. Appl. Earth Obs. Geoinf.* **2024**, *127*, 103655. [CrossRef]
83. Yuan, W.; Meng, Y.; Li, Y.; Ji, Z.; Kong, Q.; Gao, R.; Su, Z. Research on rice leaf area index estimation based on fusion of texture and spectral information. *Comput. Electron. Agric.* **2023**, *211*, 108016. [CrossRef]
84. Kelsey, K.; Neff, J. Estimates of aboveground biomass from texture analysis of Landsat imagery. *Remote Sens.* **2014**, *6*, 6407–6422. [CrossRef]
85. Mishra, P.; Nordon, A.; Asaari, M.S.M.; Lian, G.; Redfern, S. Fusing spectral and textural information in near-infrared hyperspectral imaging to improve green tea classification modelling. *J. Food Eng.* **2019**, *249*, 40–47. [CrossRef]
86. Pizarro, S.; Pricope, N.G.; Figueroa, D.; Carbajal, C.; Quispe, M.; Vera, J.; Alejandro, L.; Achallma, L.; Gonzalez, I.; Salazar, W.; et al. Implementing cloud computing for the digital mapping of agricultural soil properties from high-resolution UAV multispectral imagery. *Remote Sens.* **2023**, *15*, 3203. [CrossRef]
87. Kalecinski, N.I.; Skakun, S.; Torbick, N.; Huang, X.; Roger, J.; Vermote, E. Crop yield estimation at different growing stages using a synergy of SAR and optical remote sensing data. *Sci. Remote Sens.* **2024**, *10*, 100153. [CrossRef]
88. Dudek, G. A comprehensive study of random forest for short-term load forecasting. *Energies* **2022**, *15*, 7547. [CrossRef]
89. Tursunalieva, A.; Alexander, D.L.J.; Dunne, R.; Li, J.; Riera, L.; Zhao, Y. Making sense of machine learning: A review of interpretation techniques and their applications. *Appl. Sci.* **2024**, *14*, 496. [CrossRef]

90. Rufaioğlu, S.B.; Bilgili, A.V.; Savaşlı, E.; Özberk, İ.; Aydemir, S.; Ismael, A.M.; Kaya, Y.; Matos-Carvalho, J.P. Sensor-based yield prediction in durum wheat under semi-arid conditions using machine learning across Zadoks growth stages. *Remote Sens.* **2025**, *17*, 2416. [CrossRef]
91. Sarkar, S.; Osorio Leyton, J.M.; Noa-Yarasca, E.; Adhikari, K.; Hajda, C.B.; Smith, D.R. Integrating remote sensing and soil features for enhanced machine learning-based corn yield prediction in the southern US. *Sensors* **2025**, *25*, 543. [CrossRef] [PubMed]
92. Du, K.-L.; Jiang, B.; Lu, J.; Hua, J.; Swamy, M.N.S. Exploring kernel machines and support vector machines: Principles, techniques, and future directions. *Mathematics* **2024**, *12*, 3935. [CrossRef]
93. Toche Tchio, G.M.; Kenfack, J.; Kassegne, D.; Menga, F.-D.; Ouro-Djobo, S.S. A comprehensive review of supervised learning algorithms for the diagnosis of photovoltaic systems, proposing a new approach using an ensemble learning algorithm. *Appl. Sci.* **2024**, *14*, 2072. [CrossRef]
94. Hosmer, D.W., Jr.; Lemeshow, S.; Sturdivant, R.X. *Applied Logistic Regression*, 3rd ed.; Wiley: Chichester, UK, 2013. [CrossRef]
95. Killeen, P.; Kiringa, I.; Yeap, T.; Branco, P. Corn grain yield prediction using UAV-based high spatiotemporal resolution imagery, machine learning, and spatial cross-validation. *Remote Sens.* **2024**, *16*, 683. [CrossRef]
96. Wang, Y.; Zhang, Q.; Yu, F.; Zhang, N.; Zhang, X.; Li, Y.; Wang, M.; Zhang, J. Progress in research on deep learning-based crop yield prediction. *Agronomy* **2024**, *14*, 2264. [CrossRef]
97. Lin, Y.; Li, S.; Duan, S.; Ye, Y.; Li, B.; Li, G.; Lyv, D.; Jin, L.; Bian, C.; Liu, J. Methodological evolution of potato yield prediction: A comprehensive review. *Front. Plant Sci.* **2023**, *14*, 1214006. [CrossRef]
98. Bahrami, H.; McNairn, H.; Mahdianpari, M.; Homayouni, S. A Meta-Analysis of Remote Sensing Technologies and Methodologies for Crop Characterization. *Remote Sens.* **2022**, *14*, 5633. [CrossRef]
99. Papoutsis, I.; Bountos, N.-I.; Zavras, A.; Michail, D.; Tryfonopoulos, C. Benchmarking and scaling of deep learning models for land cover image classification. *ISPRS J. Photogramm. Remote Sens.* **2023**, *195*, 250–268. [CrossRef]
100. Farhadpour, S.; Warner, T.A.; Maxwell, A.E. Selecting and interpreting multiclass loss and accuracy assessment metrics for classifications with class imbalance: Guidance and best practices. *Remote Sens.* **2024**, *16*, 533. [CrossRef]
101. Rahman, M.H.; Sejan, M.A.S.; Aziz, M.A.; Tabassum, R.; Baik, J.-I.; Song, H.-K. A comprehensive survey of unmanned aerial vehicles detection and classification using machine learning approach: Challenges, solutions, and future directions. *Remote Sens.* **2024**, *16*, 879. [CrossRef]
102. De Magalhães, L.P.; Rossi, F. Use of indices in RGB and random forest regression to measure the leaf area index in maize. *Agronomy* **2024**, *14*, 750. [CrossRef]
103. Zeng, L.; Peng, G.; Meng, R.; Man, J.; Li, W.; Xu, B.; Lv, Z.; Sun, R. Wheat yield prediction based on unmanned aerial vehicles-collected red–green–blue imagery. *Remote Sens.* **2021**, *13*, 2937. [CrossRef]
104. Oliveira, J.S.; Brown, H.E.; Moot, D.J. Assessing potato canopy growth and development at the individual leaf level to improve the understanding of the plant source–sink relations. *N. Z. J. Crop Hortic. Sci.* **2021**, *49*, 325–346. [CrossRef]
105. Gervais, T.; Creelman, A.; Li, X.-Q.; Bizimungu, B.; De Koeyer, D.; Dahal, K. Potato response to drought stress: Physiological and growth basis. *Front. Plant Sci.* **2021**, *12*, 698060. [CrossRef]
106. Sobejano-Paz, V.; Mikkelsen, T.N.; Baum, A.; Mo, X.; Liu, S.; Köppl, C.J.; Johnson, M.S.; Gulyás, L.; García, M. Hyperspectral and thermal sensing of stomatal conductance, transpiration, and photosynthesis for soybean and maize under drought. *Remote Sens.* **2020**, *12*, 3182. [CrossRef]
107. Breiman, L. Random forests. *Mach. Learn.* **2001**, *45*, 5–32. [CrossRef]
108. Li, H.; Yan, X.; Su, P.; Su, Y.; Li, J.; Xu, Z.; Gao, C.; Zhao, Y.; Feng, M.; Shafiq, F.; et al. Estimation of winter wheat LAI based on color indices and texture features of RGB images taken by UAV. *J. Sci. Food Agric.* **2025**, *105*, 189–200. [CrossRef] [PubMed]
109. Elsayed, S.; El-Hendawy, S.; Khadr, M.; Elsherbiny, O.; Al-Suhaibani, N.; Alotaibi, M.; Tahir, M.U.; Darwish, W. Combining thermal and RGB imaging indices with multivariate and data-driven modeling to estimate the growth, water status, and yield of potato under different drip irrigation regimes. *Remote Sens.* **2021**, *13*, 1679. [CrossRef]
110. Gómez, D.; Salvador, P.; Sanz, J.; Casanova, J.L. Potato yield prediction using machine learning techniques and Sentinel 2 data. *Remote Sens.* **2019**, *11*, 1745. [CrossRef]
111. Ullah, Z.; Alsubaie, N.; Jamjoom, M.; Alajmani, S.H.; Saleem, F. EffiMob-Net: A deep learning-based hybrid model for detection and identification of tomato diseases using leaf images. *Agriculture* **2023**, *13*, 737. [CrossRef]
112. Liu, Y.; Zeng, F.; Diao, H.; Zhu, J.; Ji, D.; Liao, X.; Zhao, Z. YOLOv8 model for weed detection in wheat fields based on a visual converter and multi-scale feature fusion. *Sensors* **2024**, *24*, 4379. [CrossRef] [PubMed]
113. Unigarro, C.; Florez, H. RGB image reconstruction for precision agriculture: A systematic literature review. In *Applied Informatics*; Florez, H., Astudillo, H., Eds.; Springer Nature: Cham, Switzerland, 2025; Volume 2236, pp. 211–227. [CrossRef]

114. Lapajne, J.; Vojnović, A.; Vončina, A.; Žibrat, U. Enhancing water-deficient potato plant identification: Assessing realistic performance of attention-based deep neural networks and hyperspectral imaging for agricultural applications. *Plants* **2024**, *13*, 1918. [CrossRef] [PubMed]
115. Min, X.; Ye, Y.; Xiong, S.; Chen, X. Computer vision meets generative models in agriculture: Technological advances, challenges and opportunities. *Appl. Sci.* **2025**, *15*, 7663. [CrossRef]